Chapter 8
Transition Metal Dichalcogenides for Biomedical Applications

Linji Gong and Zhanjun Gu

Abstract The intriguing properties of two-dimensional transition metal dichalcogenides (2D TMDs) have led to the rapid development of research on these emerging 2D inorganic graphene-like nanomaterials in various fields, such as electronic devices, sensors, catalysis, and energy storage. Recently, 2D TMDs exhibit great potentials and advantages in biological systems due to their tunable optical properties, tailorable electronic characteristics, ultrahigh surface area, versatile surface chemistry, and good biocompatibility. In this chapter, we summarize the latest progress of the use of 2D TMDs for biological applications, ranging from bioanalysis, antibacterial and wound repair, bioimaging, drug delivery, and cancer therapy to tissue engineering and medical devices. Specifically, the nanotoxicology and biosafety profiles of TMDs are reviewed to meet the concern of nanomedicine from the public and scientific community. Moreover, the current challenges and future perspectives on the development of 2D TMDs for biomedical applications are also outlined. It is expected that these promising 2D TMDs will have a great practical foundation and play an important role in next-generation biomedicine.

Keywords Transition metal dichalcogenides · Nanomaterials · Bioimaging · Nanomedicine · Nanosafety

Abbreviations

2D	Two-dimensional
2D TMDs	Two-dimensional transition metal dichalcogenides
$\cdot O^{2-}$	Superoxide radical
·OH	Hydroxyl radical

L. Gong · Z. Gu (✉)
CAS Key Laboratory for Biomedical Effects of Nanomaterials and Nanosafety, Institute of High Energy Physics, Chinese Academy of Sciences, Beijing 100049, People's Republic of China
e-mail: zjgu@ihep.ac.cn

University of Chinese Academy of Sciences, Beijing 100049, People's Republic of China
gonglj@ihep.ac.cn

N. S. Arul and V. D. Nithya (eds.), *Two Dimensional Transition Metal Dichalcogenides*,
https://doi.org/10.1007/978-981-13-9045-6_8

$^1O_2$	Singlet oxygen
BBB	Blood–brain barrier
BMSCs	Bone marrow mesenchymal stem cells
BP	Black phosphorus
BSA	Bovine serum albumin
CCK-8	Cell counting kit-8
Ce6	Chlorin e6
CpG	Cytosine-phosphate-guanine
CS	Chitosan
CT	Computed tomography
CurvIS	Curved image sensor
CVD	Chemical vapor deposition
DHE	Dihydroethidine
DOX	Doxorubicin
ECM-like	Extracellular matrix-like
EMT	Epithelial-mesenchymal transition
EPR	Enhanced permeability and retention
FA	Folic acid
FL	Fluorescent imaging
GO	Graphene oxide
GSH	Glutathione
GT	Gene therapy
HA	Hyaluronic acid
HELFs	Human embryonic lung fibroblasts
HSPs	Heat shock proteins
HU	Hounsfield units
i.t.	Intratumorally
i.v.	Intravenously
ICG	Indocyanine green
MB	Methylene blue
MRI	Magnetic resonance imaging
MTT	Methylthiazolyldiphenyltetrazolium bromide
MWT	Microwave thermal therapy
NFs	Nanoflowers
NIR	Near-infrared
NMP	*N*-methylpyrrolidone
NSC	Neural stem cell
PANI	Polyaniline
PAT	Photoacoustic tomography
PDA	Polydopamine
PEG	Polyethylene glycol
PEI	Polyetherimide
PET	Positron emission tomography
PLGA	Poly(lactic-*co*-glycolic acid)
PS	Photosensitizer

PTT	Photothermal therapy
PVP	Polyvinylpyrrolidone
QDs	Quantum dots
RES	Reticuloendothelial system
rGO	Reduced graphene oxide
ROS	Reactive oxygen species
RSV	Resveratrol
SH	Sulfhydryl
SPECT	Single-photon emission computed tomography
TBO	Toluidine blue O
Tf-SH	Thiol-functionalized transferrin

8.1 Introduction

Two-dimensional transition metal dichalcogenides (2D TMDs) with unique planar topography and versatile physicochemical properties have attracted great attention and become the hot spot of fundamental research and technological applications in recent years [1–4]. 2D TMDs consist of transition metal atoms (M) and chalcogen atoms (X) with a MX_2 stoichiometry, where M ranges from Group IVB to Group VIII (e.g., Ti, V, Mo, Ta, W, and Re), and X stands for the chalcogen (S, Se, and Te) [1, 5]. The special layered structure and various combinations of transition metals and chalcogens endow 2D TMDs with versatile properties, such as ultrahigh surface area, versatile surface chemistry, unique electronic characteristics, tunable optical properties, and good biocompatibility, all of which make these materials suitable for applications in various fields including electronic devices, sensors, catalysis, energy storage, and biomedicine [6].

The increasing demand for biomedicine and rapid growth of nanobiotechnology have catalyzed and promoted the expansion of multifunctional TMDs nanosheets in the field of biomedical application [7–13]. One of the advantages of 2D TMDs for biomedical uses may be ascribed to their easy and feasible preparation methods. To date, both top-down (e.g., mechanical exfoliation, liquid exfoliation, lithium intercalation, chemical exfoliation) and bottom-up approaches (e.g., chemical vapor deposition (CVD), hydro/solvothermal methods) have been applied to prepare almost all 2D TMDs [14–16]. Then, their ultrahigh surface area and versatile surface chemistry, such as surface atomic vacancy and surface charge, enable them to link with polymers and target molecules, and/or deliver imaging agents, drugs, genes, and photosensitizers for cancer diagnosis and therapy [17, 18]. The large surface area is propitious to decorate with biocompatible polymers and further reduce the cytotoxicity and improve the dispersibility and biocompatibility of TMDs [17, 19]. Moreover, the specific surface chemistry also helps to interact with surrounding biological molecules or cellular components for the application of antibacterial strips [20] and wound repair [21]. TMDs can act as reinforcing agents within biopolymers or scaffolds for constructing extracellular matrix-like (ECM-like) materials for tissue engineering [22]

and bone regeneration [23]. Ultrathin-layered TMDs with the super photo-absorption coefficient have been developed for the soft bio-optoelectronic device in ophthalmology [24]. Also, most of the TMDs possess high photothermal conversion efficiency in the near-infrared (NIR) region and have the potential to be a novel photothermal agent for photoacoustic tomography (PAT) imaging and phototherapy [25–27]. Some TMDs (e.g., MoS_2, WS_2, TaS_2, ReS_2) with high atomic number have been reported to be suitable for X-ray-computed tomography (CT) contrast agents [28] and radiosensitizers [29] due to their strong X-ray attenuation performance. More importantly, the toxicity and safety profiles are the first factors of concern when applying TMDs in biological applications. Researches on the toxicity profile of TMDs nanosheets show that this newly developed 2D material exhibits lower cytotoxicity than many other nanostructures [9, 10], ensuring their further applications for the direction of nanomedicine.

Here, we will summarize the latest progress of the utilization of 2D TMDs for biomedical field, ranging from bioanalysis, antibacterial and wound repair, bioimaging, diagnosis, drug delivery, and cancer therapy to tissue engineering and medical devices. Specifically, the nanotoxicology and biosafety profiles of TMDs are reviewed to meet the concern of nanomedicine from the public and scientific community. Moreover, the current challenges and future perspectives on the development of 2D TMDs for biomedical applications are also outlined.

8.2 Bioanalysis and Disease Diagnosis

Development of techniques for early and effective diagnosis of diseases is of highly desired and paramount importance. The last decade has witnessed the rapid growth of the application of TMDs in bioanalysis and disease diagnosis [30]. Owing to the versatile physiochemical properties, such as easy preparation, layered structure, large surface area, desirable optical properties, tunable electric properties, favorable catalytic properties, and good biocompatibility, TMDs nanosheets have been widely developed as fluorescent biosensors, electrochemical biosensors, photoelectrochemical biosensors, field-effect transistor (FET) biosensors, and nanopore biosensors, to fast, sensitively and selectively detect or analyze various biomolecules (e.g., DNA, RNA, glucose, cholesterol, dopamine, cholesterol, protein, antigen, enzyme, glutathione (GSH), and biomarkers) and the surrounding environment (e.g., pH, H_2O_2, ATP) and cells (e.g., cancer cells, bacteria, virus). The readers can find out the related contents of the mechanism and application of 2D TMDs-based biosensors in other chapter.

8.3 Antibacterial and Wound Repair

From ancient times, our forefathers had known that water, wine, and vinegar stored in silver-coated containers could efficiently limit bacterial contamination [31]. With the rapid development of modern medicine in the twentieth century, many antibiotics were produced to prevent bacterial infections, which led to a dramatic decline in mortality rates all over the world. However, it was unexpected that the misuse or long-term use of antibiotics gives rise to the uncertain outbreaks of infectious diseases caused by drug-resistant bacteria. Thus, we are bound to seek more efficient alternately antibacterial strategies to prevent the rise of bacterial infections.

Nanomaterials-based antibacterial agents have come into the picture in the past decade. Compared with antibiotics, nanomaterials could inhibit the growth of bacteria with various mechanisms, such as the deconstruction of cell wall/membrane, the production of reactive oxygen species (ROS), the interaction with the biological macromolecules, the interruption of electron transport, and the release of metal ions in bacteria [32, 33]. Not limited to nano-silver [33–35], TMDs nanomaterials, such as MoS_2 [36–39], WS_2 [39–42] and their composites [43–45], also show high antibacterial activity. For example, it was reported that the antibacterial ability of chemically exfoliated MoS_2 nanosheets was better than that of the untreated MoS_2 powders [36]. This phenomenon may be ascribed to the larger surface area and better electronic properties of the nanoscale MoS_2 sheet. The antimicrobial mechanisms mainly include membrane and oxidation stress caused by the increased interaction rate between MoS_2 nanosheets and bacteria and the production of ROS. Similarly, Navale et al. [41] also tested the antibacterial performances of WS_2 nanosheets against four bacterial strains through oxidative and membrane stress approaches. But they found that WS_2 did not produce ROS, which was contradictory to the case of its structural analog, MoS_2. Notably, this outcome is consistent with the later work by Liu et al. [42]. Under UV irradiation, as shown in Fig. 8.1, the phototoxicity of CdS, MoS_2 as well as WS_2 nanoparticles toward Escherichia coli (*E. coli*) was different (CdS > MoS_2 > WS_2) [39]. When exposed to the same mass concentration (such as 50 mg/L) of those three nanoparticles, the inhibition ratios of *E. coli* were 96.7, 38.5, and 31.2%, respectively. Different from the above-mentioned outcomes [41, 42], WS_2 and MoS_2 could produce ROS including superoxide radical ($\cdot O^{2-}$), singlet oxygen ($^1O_2$), and hydroxyl radical (·OH) under UV irradiation [39], while CdS generated only $\cdot O^{2-}$ and $^1O_2$ [39]. In addition, due to the photon energy (3.4 eV) of the incident UV light is higher than the band gap of WS_2 (2.1 eV) and CdS (2.5 eV), the photocorrosion process will appear: $WS_2 + 6h^+ \xrightarrow{hv} W^{6+} + 2S$. Moreover, under the irradiation of UV light, CdS and WS_2 could release metal ions, but no detectable amount of Mo ion was found [39]. Thus, the dominant antibacterial mechanism of MoS_2 may be ascribed to the generation of ROS, while both ROS production and toxic metal ions release contribute to the toxic mechanism of CdS and WS_2. In addition, some TMDs-based nanocomposites also have been fabricated to further increase the antibacterial activity. For example, Navale et al. [41] found that reduced graphene oxide (rGO) and WS_2 were not able to produce $\cdot O^{2-}$ or ROS but

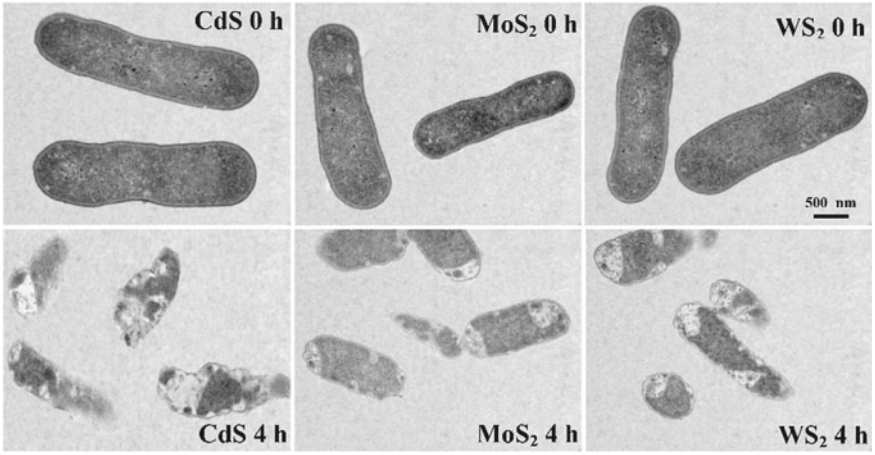

Fig. 8.1 Antibacterial ability of CdS, MoS_2, and WS_2. TEM micrographs of *E. coli* cells exposed to three sulfide nanoparticles before and after 4 h UV irradiation. (Reprinted with permission from Ref. [39]. Copyright 2017, Elsevier.)

the rGO-WS_2 composite could generate both. It was shown that the higher antibacterial effects were observed in the group of rGO-WS_2 nanocomposite than solo WS_2 or rGO.

The antibacterial properties of TMDs give them the opportunity to play a role in antimicrobial therapy. For example, Yin et al. [21] fabricated a versatile antibacterial agent based on polyethylene glycol (PEG) modified MoS_2 nanoflowers (PEG-MoS_2 NFs) for safe and synergetic wound antibacterial applications. Firstly, the PEG-MoS_2 NFs with good biocompatibility can be easily uptaken by cells. Second, the peroxidase-like activity enables it to efficiently catalyze H_2O_2 to produce cytotoxic ·OH, which has a higher antibacterial capacity. Besides, PEG-MoS_2 NFs with a large surface area and high NIR absorption will be propitious to further improve the bacteria-killing effects by NIR-induced hyperthermia. In mice model, the PEG-MoS_2 NFs and low concentration of H_2O_2 solutions were dropped on the wound area of mice after bacterial infection. The wound-healing results demonstrated that the PEG-MoS_2 NFs with peroxidase catalytic and NIR absorption capacities could significantly inhibit the growth of resistant bacteria in wounds. Similarly, Huang et al. [46] also found that silk fibroin-modified $MoSe_2$ nanosheets with low cytotoxicity and favorable peroxidase-like ability showed rapid wound-healing efficacy in vivo. Different from Yin's work [21], silk fibroin-$MoSe_2$ films were posted on the skin of infection area. Cao et al. [20] also designed an efficient and benign antibacterial depot by the integration of Ag^+ and MoS_2 nanosheets. Compared with an equal amount of $AgNO_3$, the depot showed higher broad-spectrum antibacterial ability due to the efficient release of Ag^+. In addition, the antibacterial system exhibited negligible biotoxicity, high antibacterial activities and avoided the waste of Ag. Besides wound bacterial infection, artificial implants also provide a hospitable place for bacterial

adherence and growth. Therefore, it is necessary to develop new-style multifunctional artificial implants with excellent self-antibacterial capabilities. Feng et al. [47] fabricated Ti implant coated with chitosan-assisted MoS_2 ($CS@MoS_2$) hybrid via electrophoretic deposition. The implant exhibited significantly antibacterial efficacy under the combined irradiation of 660 and 808 nm light than the irradiation separately, which might stem from the synergistic function of both $^1O_2$ and hyperthermia. After the implantation of $CS@MoS_2$-Ti in mice, the photodynamic process can produce ROS under 660 nm visible light while the photothermal process will enhance the temperature of the Ti implants when exposed to an 808 nm light. This research demonstrated that TMDs-based artificial implants with novel self-antibacterial abilities showed great promising for in situ disinfection.

8.4 Bioimaging

Over the past decades, TMDs have emerged as promising candidates in bioimaging and diagnosis due to their versatile physicochemical properties including layered structure, tunable band gaps, fluorescence properties, and low cytotoxicity. On the one hand, TMDs can be used as imaging agents for diagnosis or imaging-guided therapy, which have been illustrated with many works in recent years. On the other hand, and more importantly, molecular imaging technologies, such as fluorescent imaging (FL), PAT imaging, CT imaging, positron emission tomography (PET) imaging, and single-photon emission computed tomography (SPECT) imaging, can be applied to monitor the in vivo tracking, biodistribution, transportation, and clearance processes of TMDs nanoparticles to meet the concern of drug delivery and nanosafety.

8.4.1 Fluorescent Imaging

Compared with the traditional organic fluorescent molecule, semiconductor quantum dots (QDs) with tunable wavelength, good photostability, and high quantum yields throw light on the development of in vivo bioimaging [7, 48–51]. Nevertheless, the cellular toxicity of traditional inorganic QDs (such as cadmium-containing QDs) severely restricts its biomedical applications [52]. Therefore, it is highly significant to develop newly fluorescent nanomaterial. The emerging TMDs with easily tunable structures and optical properties plus good compatibility show alternative potential application for fluorescent bioimaging. Firstly, the large surface area and versatile surface chemistry of TMDs will enable them to be good fluorescein carriers. For examples, Cy5.5-labeled WS_2-$Fe_3O_4@SiO_2$-PEG [53] or BSA-MoS_2 [54] can be applied for in vivo NIR fluorescence imaging to realize the visualization and localization of the biodistribution of the nanocomposite in the small animal. Compared with TMDs nanosheets, 0D TMDs QDs (e.g., MoS_2 QDs) with lateral sizes less than 10 nm show unique optical and electrical properties for their stronger quantum con-

finement and edge effects [55–57]. For instance, the monodispersed MoS_2 QDs with different uniform lateral diameters of ~3.5 nm [55], ~2.9 nm [56], and ~2.6 nm [57] show fluorescence quantum yield of 9.65, 3.1, and 5.6% and fluorescence lifetime of 4.66, 11.0, and 12 ns, respectively. Those optical features suggest that the MoS_2 QDs is suitable for the applications of bioanalysis and cellular bioimaging.

8.4.2 Photoacoustic Tomography Imaging

PAT imaging is a newly developed noninvasive diagnostic imaging technology based on the photoacoustic effects in biological tissue [58]. Compared with the traditional optical imaging modality, this emerging PAT imaging offers remarkably increased penetration depth and spatial resolution [59]. Therefore, PAT imaging may be contributed to study the in vivo tracking of nanoparticles.

Based on the excellent NIR-absorbance performance and strong photothermal effects, TMDs can produce thermal signals by thermal expansion or bubble formation [27], which enables their suitability for PAT imaging. For example, one of the first explorations of TMDs-based PAT imaging was published by Cheng et al. [59]. They used WS_2-PEG nanosheets as a photoacoustic agent to display its tumor accumulation by the degree of photoacoustic signals. When the tumor-bearing mice were intratumorally (i.t.) injected with the as-prepared WS_2-PEG (2 mg/mL, 20 μL) and subsequently imaged at different time points, strong photoacoustic signals in the tumor region could be detected to show and visualize the efficient accumulation of WS_2-PEG nanosheets in tumor through the enhanced permeability and retention (EPR) effect. After that, for the sake of the easy-to-fabricate feature and effective NIR light-to-heat conversion capability, various TMDs with different morphology and components (e.g., MoS_2 nanosheets [54, 60–66], MoS_2 nanodots [67–69], $MoSe_2$ nanosheets [70, 71], WS_2 nanosheets [72, 73], WS_2 nanodots (Fig. 8.2) [74], TiS_2 nanosheets [75], VS_2 nanosheets [76], ReS_2 nanosheets [77, 78], MoS_2 or WS_2-based nanocomposites [79–82], and some ternary chalcogenide nanosheets (Cu_2MnS_2 [83] and Ta_2NiS_5 [84]) have also been developed for PAT imaging applications.

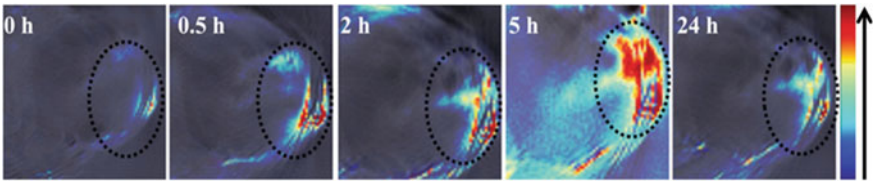

Fig. 8.2 TMDs-based photoacoustic tomography imaging. PAT images of tumor before and after intravenously (i.v.) injection with WS_2@PEI nanoparticles at various time points. (Reprinted with permission from Ref. [74]. Copyright 2016, Wiley-VCH.)

8.4.3 Computed Tomography Imaging

X-ray CT imaging is a well-established biomedical imaging technique being routinely used in various researches and clinical diagnosis [9, 28]. CT imaging is a non-invasive bioimaging tool which provides a 3D visual reconstruction of the targeted tissues with deep penetration and high resolution [9]. In CT imaging, the weakness X-ray contrast signals can be enhanced and amplified by the use of contrast agents [9, 59]. As a rule, the X-ray absorption coefficient (μ) is formalized as follows: $\mu = \left(\rho Z^4\right)/\left(AE^3\right)$, where A is the atomic mass and E is the X-ray energy [28]. Therefore, CT contrast agents possessing higher density (ρ) or high atomic number (Z) tend to have stronger X-rays absorbability.

As with gold and lanthanides nanoparticles-based CT imaging agents [28], TMDs that comprise high atomic number metal elements (e.g., Mo, Ta, W, Re; their atomic number is 42, 73, 74, and 75, respectively) have also been reported to be suitable for CT imaging in recent years. For example, PEG [53, 59, 72, 85, 86], BSA [87], PEI [74], hyaluronic acid (HA) [88], or polyvinylpyrrolidone (PVP) [73] modified biocompatible WS_2 nanosheets or nanodots was successfully prepared for in vitro and in vivo CT imaging. The X-ray attenuation coefficient of the W atom at 100 keV is 4.438 cm^2/kg, which is higher than that of iodine (1.94 cm^2/kg at 100 keV) [85]. WS_2 shows higher Hounsfield units (HU) value indeed when compared with commercial iodine-based clinic used contrast agents (e.g., Iohexol [85], Iobitridol [73], Iopromide [59, 86, 87]) at the same concentration in those works. It is noted that the widely used small molecular CT contrast agent, such as Iobitridol, can be rapidly cleared from the blood within minutes [89]. Therefore, biocompatible nanoscale materials-based CT contrast agents may have significant advantages compared with those traditional iodine-based small molecular contrast agents.

The excellent CT contrast ability in vitro of WS_2 nanosheets encouraged researchers further to pursue their in vivo CT imaging applications. For example, BEL-7402 tumor-bearing mice were i.v. injected with PEGylated WS_2 QDs solution (15 mg/mL, 200 μL) and then time-dependent whole-body CT imaging was collected [86]. Before administration of WS_2-PEG nanoparticles, the CT signals of the liver, spleen, and tumor region were very weak, as shown in Fig. 8.3. In contrast, we could observe the obvious enhancement of contrast signals in liver and spleen after i.v. injection, suggesting the uptake of WS_2-PEG nanoparticles by the reticuloendothelial system (RES). After 2 h post-injections, the remarkably enhanced contrast signals in tumorous regions were detected, which could be contributed to the gradual accumulation of nanoparticles in tumors through passive targeting approach. Additionally, the contrast signals in the bladder were also gradually enhanced, indicating that the ultrasmall WS_2 QDs might be cleared out through renal filtration and own better biocompatible and biodegradable properties. Similarly, polymer functionalized ReS_2 [77, 78] and TaS_2 [89] nanosheets also can act as promising contrast agents for CT bioimaging due to the strong X-ray attenuation performance of Re and Ta. Besides, TMDs can conjugate with other components such as Au [90], Bi_2S_3 [79] or doped with Gd^{3+} ion [71, 72, 91] to realize better CT imaging effects. Those

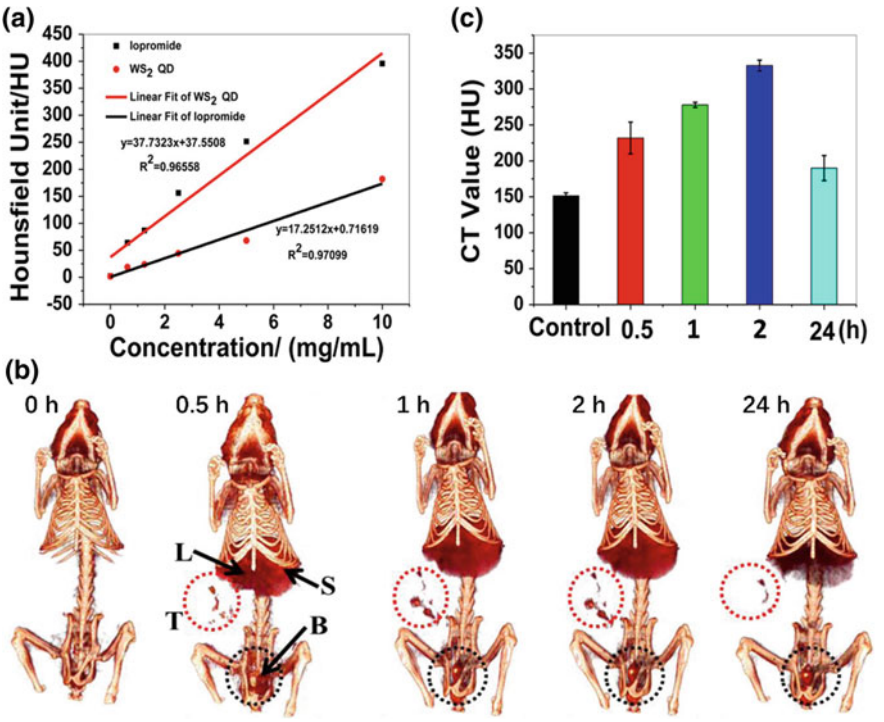

Fig. 8.3 TMDs-based computed tomography imaging. **a** Hounsfield unit values of iopromide and WS_2 QDs. **b** CT images of tumor before and after i.v. injection of WS_2 QDs solution at different time points. **c** Corresponding HU value of CT images. (Adapted with permission from Ref. [86]. Copyright 2015, American Chemical Society.)

examples demonstrated that CT imaging could be applied to investigate the in vivo biodistribution, transportation, and clearance processes of nanoparticles to realize multifunction of nanomedicine.

8.4.4 Multimodal Imaging

It is worth noting that each imaging modality has its own advantages and drawbacks. Therefore, the development of novel "all-in-one" bioimaging agents to combine different imaging modalities is of highly desired and full of promising.

With the repaid development of molecular imaging, nanoparticles-based multimodal bioimaging has become a booming trend. On the one hand, the inherent excellent NIR-absorbance performance and strong X-ray attenuation ability endow some TMDs with dual-modal PAT and CT imaging capability, to integrate the advantages of CT and PAT imaging. For example, Miao et al. [78] prepared colloidal

ReS_2 nanosheets by liquid exfoliation method for in vivo PAT and CT imaging. The obtained PVP-ReS_2 nanosheets possess excellent photothermal conversion efficiency (79.2%), which is higher than those of MoS_2 (24.37%) [92] and WS_2 (32.83%) [87]. The photoacoustic signals in the tumorous region were significantly enhanced and reached the strongest at around 1 h after i.v. injection, indicating the efficient accumulation of ReS_2 nanosheets via the EPR effect. In addition, the ReS_2 nanosheets are also suitable for the application of CT imaging. When the tumor-bearing mice were i.t. injected with PVP-ReS_2 solutions (10 mg/mL, 50 μL), an obvious contrast signal enhancement of the tumorous region was detected. Hence, the ReS_2 nanosheets and other TMDs such as MoS_2 [68, 79], $MoSe_2$ [93], WS_2 [59, 68, 73, 74, 86, 88] with inherent versatile imaging capability can serve as a multifunctional contrast agent for both PAT and CT imaging. On the other hand, some functional moieties (e.g., magnetic particle, radioisotope), with other imaging capabilities, can be modified onto the surface of 2D TMDs to realize multimodal bioimaging. As mentioned above, PAT imaging provides useful information on in vivo tracking and biodistribution of nanoparticles inside the tissue, while magnetic resonance imaging (MRI) possesses high spatial resolution and excellent soft-tissue contrast effects with a noninvasive feature. Thus, the combination of PAT and MRI imaging will further improve the ability of diagnostic imaging. For example, Chen et al. [76] for the first time found that PEGylated VS_2 nanodots could be used for T1-weighted MRI and PAT imaging-guided photothermal therapy (PTT) due to its paramagnetism and high NIR-absorbance feature. Meanwhile, there are many works reporting that iron oxide (IO) [53, 62, 80, 81, 94–97] or Gd^{3+} ion [63, 71, 72, 91, 98] modified TMDs can serve as dual-modal contrast agents for PAT and MRI imaging. Liu et al. [62] successfully prepared iron oxide-decorated MoS_2 nanosheets via a sulfur chemistry strategy to form MoS_2-IO-PEG composites, which possess both the superparamagnetic feature and T2 contrast capability. All the tumors and livers of mice after 24 h post-injection of MoS_2-IO-PEG exhibited obvious darkening effects in T2-weighted MRI images when compared to untreated mice. The results showed the effective aggregation of MoS_2-IO-PEG nanocomposites in tumors. Pan et al. [71] fabricated Gd^{3+}-doped $MoSe_2$ nanosheets via a simple liquid phase method and then employed this $MoSe_2(Gd^{3+})$-PEG nanosheets as a theranostic agent for PAT and MRI dual-modal bioimaging and PTT. In a similar work, Gd^{3+} ions were used to enhance the contrast action of WS_2 nanosheets in both MRI and CT imaging and also further increased the efficacy of radiotherapy [72]. 2D TMDs nanosheets also can be easily modified with radioisotope tracer including ^{64}Cu [62, 99], ^{188}Re [100], ^{89}Zr [101], and $^{99m}Tc^{4+}$ [76, 77] to enable noninvasive nuclear imaging such as PET and SPECT imaging. For instance, $^{99m}Tc^{4+}$ ions, as a wide clinic used radioisotope tracer, could be firmly and efficiently anchored on the surface of VS_2 nanosheets through a chelator-free labeling strategy [76]. The signals of in vivo tumor SPECT imaging were gradually increased from time after the i.v. injection of ^{99m}Tc-VS_2@lipid-PEG, indicating the timely accumulation of nanoparticles by EPR effect. The delivery efficiency of ^{99m}Tc-VS_2@lipid-PEG was calculated up to 5.1 ± 1.2% ID/g at 24 h [76]. It was demonstrated that nuclear imaging could help to precisely reveal the biodistribution and tracking in vivo of administrated nanoparticles. In a word, taking full

advantages of the high NIR and X-ray absorbance capabilities and functionalized by magnetic components or radioisotope tracer, TMDs can serve as an "all-in-one" nanoplatforms for multimodal in vivo tumor imaging including PA, CT, MRI, PET, and SPECT imaging and imaging-guided therapy (Table 8.1).

8.5 Cancer Therapy

8.5.1 Photothermal Therapy

PTT is an invasive therapeutic modality, which typically employs external laser (usually NIR light) to cause hyperthermia within tumor tissues. Hyperthermia (41–43 °C) can effective thermal ablate cancer cells via the change of the tumor microenvironment, induction of apoptosis, and induction of gene and protein synthesis [108]. PTT also causes serious side effects to surrounding normal tissues. Moreover, PTT is often hard to completely ablate the deep-located cancer cells due to the insufficient penetration of laser. Thus, 2D TMDs nanosheets with better NIR light absorbance property and excellent photothermal conversion performance will bring about an alternative and feasible solution for promoting the efficiency of PTT.

In 2013, it was reported that MoS_2 nanosheets exhibited better photothermal performance than that of Au and graphene and thus can be used as NIR photothermal agents [109]. The MoS_2 nanosheets were chemically exfoliated via the Morrison method. The as-prepared MoS_2 nanosheets have a mass extinction coefficient up to 29.2 L/(g cm) at 800 nm, which is approximately 7.8-fold of graphene oxide [3.6 L/(g cm)] [109] higher than that of gold nanorods [13.89 L/(g cm)] [110]. The in vitro photothermal experiment showed better HeLa cells killing efficacy when incubated with MoS_2 and subsequently treated with NIR irradiation (800 nm, 20 min). After that, the application of TMDs in the field of PTT has exponentially increased. For example, Wang et al. [111] for the first time used a versatile "bottom-up" one-pot synthesis method to successfully synthesize PEGylated MoS_2 nanosheets for highly efficient PTT. Ultrathin MoS_2 nanosheets with a smaller diameter were prepared via the solvothermal procedure, which is very different from traditional "up-down" strategy via exfoliation from bulk MoS_2 [59, 92, 109]. The $(NH_4)_2MoS_4$ was utilized as a novel precursor to synchronously provide both Mo and S sources, and PEG-400 aqueous solution was used as the solvent to control the size and enhance the colloidal stability and biocompatibility of MoS_2 nanosheets. The as-prepared MoS_2 nanosheets with no significant cytotoxicity were confirmed by in vitro cell viability assay of 4T1 cells incubated with nanosheets, even at the concentration up to 500 μg/mL. Encouraged by the better in vitro photothermal cells killing performance, MoS_2 nanosheets also exhibits excellent antitumor efficiency in vivo, demonstrating MoS_2 nanosheets have a great potential for PTT.

Like MoS_2, WS_2 nanosheet is another representative example of the TMDs family and also shows promising NIR photothermal agents. Cheng et al. [59] synthesized

Table 8.1 The applications of 2D TMDs for bioimaging and cancer therapy

TMD	Modification	Bioimaging	Therapy	References
TiS_2	PEG	PAT	PTT	[75]
VS_2	PEG, $^{99m}Tc^{4+}$	PAT/MRI/SPECT	PTT	[76]
MoS_2	BSA, Gd^{3+}	PAT/MRI	PTT	[63]
	^{64}Cu, Fe_3O_4, PEG	PAT/MRI/PET	PTT	[62]
	BSA		MWT	[102]
	mPEG-PLGA, DOX, Fe_3O_4	CT/MRI	MWT/chemotherapy	[95]
	PEG, Ce6	PAT	PTT/PDT	[61]
	BSA	FL/PAT	PTT/PDT	[54]
	PEG, DOX		PTT/chemotherapy	[103]
	Chitosan, DOX	CT	PTT/chemotherapy	[92]
	PEI, HA, DOX	PET	PTT/chemotherapy	[99]
	Fe_3O_4, ICG, Pt(IV), PEI	PAT/MRI	PTT/PDT/chemotherapy	[81]
	PEG, CpG		PTT/immunotherapy	[104]
	PANI, PEG	PAT/CT	PTT/RT	[68]
	Bi_2S_3, PEG	PAT/CT	PTT/RT	[79]
$MoSe_2$	BSA, ICG	PAT	PTT	[70]
	PEG, Gd^{3+}	PAT/MRI	PTT	[71]
	PDA, DOX		PTT/chemotherapy	[105]
TaS_2	PEG, DOX	CT	PTT/chemotherapy	[89]
WS_2	PEG	PAT/CT	PTT	[59]
	PVP	PAT/CT	PTT	[73]
	BSA, MB	CT	PTT/PDT	[87]
	Fe_3O_4, PEG, DOX	FL/CT/MRI	PTT/chemotherapy	[53]
	PEI, siRNA	PAT/CT	PTT/gene therapy	[74]
	LA-PEG	PAT/CT	PTT/RT	[86]
	PEG, ^{188}Re	SPECT	PTT/RT	[100]
	PEG, Gd^{3+}	PAT/CT/MRI	PTT/RT	[72]
	Fe_3O_4, $sSiO_2$, MnO_2, PEG	FL/PAT/MRI	PTT/RT	[97]
	HA, PANI, Ce6	FL/PAT/CT	PTT/PDT/RT	[88]
WSe_2	BSA, MB		PTT/PDT	[106]
ReS_2	PVP	PAT/CT	PTT	[78]
	BSA, RSV, FA		PTT/chemotherapy	[107]
	PEG, $^{99m}Tc^{4+}$	PAT/CT/SPECT	PTT/RT	[77]

MB methylene blue; *BSA* bovine serum albumin; *RSV* resveratrol; *FA* folic acid; *PVP* polyvinylpyrrolidone; *PDA* polydopamine; *PLGA* poly($_{D,L}$-lactide-*co*-glycolide acid); *ICG* indocyanine green; *HA* hyaluronic acid; *PANI* polyaniline; *Ce6* chlorin e6; *CpG* cytosine-phosphate-guanine; *MWT* microwave thermal therapy; *Tf-SH* thiol-functionalized transferrin

PEGylated WS_2 nanosheets with strong NIR-absorbance performance for in vivo CT and PAT imaging-guided PTT. The WS_2-PEG nanosheets with the diameter of 50-100 nm and thickness of ~1.6 nm were revealed by TEM and AFM, respectively. The mass extinction coefficient of the as-prepared PEGylated WS_2 nanosheets was calculated to be 23.8 L/(g cm) at 808 nm. Compared to the uncoated WS_2 nanosheets, PEGylated WS_2 nanosheets have better biocompatibility with no significant cytotoxicity, making it suitable for further biomedicine application. The excellent in vivo photothermal antitumor outcome was achieved in the group of treated with WS_2-PEG solution (2 mg/kg of i.t. injection, 20 μL) and NIR laser (808 nm, 0.8 W/cm^2, 5 min). The tumor surface temperatures rapidly increased from ~30 to ~65 °C within 5 min. As a result, the treated tumors have been completely inhibited without obvious reoccurrences and the mice survived over 45 days. The PVP-ReS_2 nanosheets with ultrahigh photothermal conversion efficiency (79.2%) were also found to remarkable ablate and eradicate the tumors without recurrence [78]. In addition, Li et al. [112] were the first to discover that chemically exfoliated WS_2 nanosheets could not only efficiently inhibit Aβ aggregation due to the selective adsorption of Aβ monomers on the surface of WS_2 nanosheets through van der Waals and electrostatic interactions but also cross the blood–brain barrier (BBB) and dissociate preformed Aβ aggregates upon NIR irradiation. Moreover, a similar work further confirmed the inhibition of Aβ aggregation by MoS_2 and found that MoS_2 nanoparticles could block the Aβ-formed Ca^{2+} channel and maintain the calcium homeostasis [113]. These phenomena will open a new avenue for PTT of Alzheimer's disease and enlarge the biological application fields of WS_2 nanosheets.

The photothermal conversion efficiency of many TMDs (such as those mentioned above, MoS_2 [109] and WS_2 [59]) was experimentally investigated only based on the optical part and described by the mass extinction coefficient, which reflects the wavelength-selective absorbing feature and the absorbance capability of nanoparticles [78, 114]. However, the photothermal conversion performance of an agent mainly depends on two independent factors: the mass extinction coefficient (ε) and photothermal conversion efficiency (η) [78, 115]. Photothermal conversion efficiency often represents the ability of the conversion from light energy to heat energy [78]. Therefore, many works also studied the photothermal conversion efficiency of TMDs, which was shown in Table 8.2. For example, $MoSe_2$ nanosheets have revealed a photothermal conversion efficiency of 57.9% [116], which is higher than that of MoS_2 (24.37%) [92], Nb_2C nanosheets (36.4%) [115], Ta_4C_3 nanosheets (44.7%) [117], black phosphorus (BP) QDs (28.4%) [118], and Au nanorods (21%) [119–121]. Besides the typical MoS_2 [23, 62–64, 67, 69, 80, 109, 111, 122–133] and WS_2 [73, 85, 134–136], many other TMDs (e.g., $MoSe_2$ [70, 71, 93, 116, 132, 137, 138], TiS_2 [75, 139], SnS [140], VS_2 [76], ReS_2 [78]) with different component and surface chemistry also have been demonstrated as efficient NIR light-driven agents for PTT.

Although the TMDs-based photothermal agents have achieved remarkable antitumor efficacy in PTT, some heat-resistant cancer cells are hard to be eradicated by PTT alone. It is infeasible to directly increase the laser power, which will inevitably damage to the surrounding healthy tissue. On account of the heat resistance of cancer cells stem from the intrinsic heat shock response, we can develop novel strategies

Table 8.2 The photothermal conversion performance of various agents including traditional photothermal agents and novel 2D nanomaterials

Material	Photothermal conversion efficiency (η, %)	Mass extinction coefficient [ε, L/(g cm)]	Wavelength (λ, nm)	References
TiS_2	–	26.8	808	[75]
VS_2	31.5	22.6	808	[76]
MoS_2	24.37	29.2	808	[92, 109]
$MoSe_2$	57.9	11.1	808	[116]
$MoTe_2$	33.8	3.15	808	[141]
SnS	36.1	16.2	808	[140]
TaS_2	39	–	808	[89]
WS_2	32.83	21.8	808	[87]
WSe_2	35.07	–	808	[106]
ReS_2	79.2	4.35	808	[78]
Ti_3C_2	30.6	25.2	808	[142]
Nb_2C	36.4	37.6	808	[115]
Ta_4C_3	44.7	4.06	808	[117]
Ta_2NiS_5	35	25.6	808	[84]
Bi_2Se_3	34.6	11.5	808	[143]
BP QDs	28.4	14.8	808	[118]
Nano-rGO	–	24.6	808	[144]
Au nanorods	21	13.9	808	[120]

to inhibit the production of heat shock proteins (HSPs) (such as Hsp70 and Hsp90) by regulating the related genes expression [74, 126, 145, 146]. For example, Zhang et al. [74] decorated a positively charged polyetherimide (PEI) onto the surface of MoS_2 to efficient carrying negatively charged survivin-siRNA. Firstly, hyperthermia could increase cell membrane permeability and thus enhance the cellular uptake of the as-prepared WS_2@PEI-siRNA nanocomposite. Then, the silencing of survivin could downregulate the Hsp70 expressions, making heat-resistant cancer cells more susceptible to PTT. As a result, all the WS_2@PEI-siRNA involved in vitro and in vivo experiments showed a remarkable synergistic GT/PTT efficacy (Fig. 8.4). Besides the regulation of genes expression by loading siRNA onto WS_2, using protein inhibitor to disturb the function of Hsp90 also a feasible approach to enhance PTT efficacy. Ariyasu and Mu et al. [126] utilized CS@MoS_2 as a carrier to load cyclic peptide sequence (Cype), which could specifically bind to N-middle domain of intracellular Hsp90. The as-prepared CS@MoS_2-Cype nanocomposite could effectively induce tumor ablation through the process of necrosis and enhance apoptosis under 808 nm NIR light irradiations, resulting in significant enhancement of photothermal treatment.

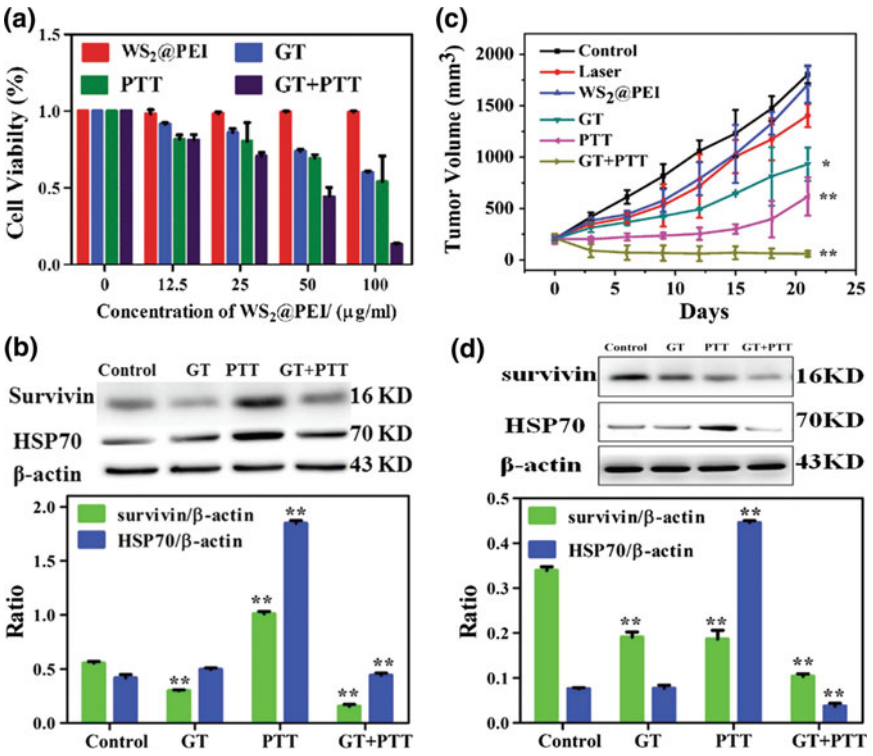

Fig. 8.4 TMDs-based PTT/GT combination therapy. **a** Photothermal effect of WS_2@PEI-siRNA on BEL-7402 cells. **b** The protein expressions of survivin and HSP70 of BEL-7402 cells from different treatments for 24 h. **c** Tumor volume growth curves of mice after combined PTT/GT therapy. **d** The protein expression levels of survivin and HSP70 of tumors from different groups. (Reprinted with permission from Ref. [74]. Copyright 2016, Wiley-VCH.)

8.5.2 Microwave Thermal Therapy

The employ of nanomaterials to induce localized heating within tumor tissue for the thermal ablation of cancer cells is a general strategy in nanomedicine, mainly including three approaches: the absorption of NIR light, magnetically induced heating, and radiofrequency ablation [147]. In the above-mentioned section, we can conclude that the applications of TMDs in PTT usually rely on the external incident light, especially the NIR light due to the strong absorption by agents, high tissue penetration depths, and low absorption of hemoglobin and water in the region around 650–900 nm [148]. In the photothermal process, light induces the generation of hyperthermia to ablate cancer cells. Different from light-mediated PTT, the hyperthermia situations in microwave thermal therapy (MWT) are triggered by external radiofrequency (microwave) irradiation. The clinic translation of PTT is limited by the penetration depths of NIR light (typically 1–3 mm [149]), while microwave possesses a deeper

tissue penetration, faster heat generation, and wider ablation zones [102]. Moreover, the microwave has been proofed as a friendly heat source to be applied for tumor ablations in clinical [95, 150].

Recently, TMDs have also been found to be suitable for MWT. For example, Wang et al. [102] successfully synthesized layered MoS_2 NFs via a hydrothermal process for cancer MWT for the first time. The MoS_2 NFs was then modified by bovine serum albumin (BSA) to improve its biostability and biocompatibility. The average temperature of solutions was rapidly increased to as high as 42 °C after treated with microwave (1.8 W, 450 MHz) for 1 min and 53 °C for 5 min. In the animal experiment, ICR mice were i.t. injected with BSA-MoS_2 NFs (20 mg/kg) and then irradiated by microwave for 5 min in the tumor region after two hours injection. Tumors on mice were completely eliminated after microwave treatment, preliminary demonstrating the as-prepared layered BSA-MoS_2 NFs have the potentials to be promising microwave hyperthermia sensitizers for cancer MWT. After that, Tang and Fu et al. [95] developed biocompatible mPEG-PLGA microcapsules with doxorubicin (DOX) hydrochloride (DOX·HCl), MoS_2 nanosheets and Fe_3O_4 nanoparticles encapsulated for MRI/CT dual-modal imaging-guided microwave-induced tumor therapy. These microcapsules possess at least seven advantages include: (1) easy to prepare; (2) hybrid organic-inorganic composites, biocompatible, degradable, and no significant toxicity; (3) superselective arterial blocking; (4) superior microwave sensitive property; (5) controlled release DOX·HCl under the microwave irradiation; (6) in vivo MRI/CT dual-modal imaging; (7) synergetic chemotherapy and MWT. Following up this work, the same research group [151] performed a systematic study of MoS_2-mediated microcapsules (MSMC)-based microwave embolization agents for large orthotopic transplantation tumor therapy. To eradicate the large orthotopic transplantation tumor, a novel microwave embolization agent was prepared by enclosing MoS_2 nanosheets in the sodium alginate microcapsules. This agent not only has a good biocompatibility and body-clearable but also exhibits excellent embolic and microwave susceptible properties. Moreover, as shown in Fig. 8.5, microcapsules can be dispersed in the margin of tumors after the arterial injection and then induce the embolic effect on the blood vessels, which remarkably increases the microwave ablation efficiency by reducing heat loss and cutting off the feeding of nutrition [151]. The results show that the ablation zone was enlarged 5 times compared to the microwave alone group. The excellent antitumor efficacy was contributed to the synergistic therapy of enhanced MWT and transcatheter arterial embolization.

8.5.3 Photodynamic Therapy

Photodynamic therapy (PDT) is a clinically approved, minimally invasive therapeutic method [152]. PDT procedure requires three important components: photosensitizer (PS), light, and oxygen [152]. In the presence of oxygen and under light irradiation, the administrated photosensitizing molecules absorb the light energy to produce toxic ROS (e.g., $^1O_2$) to kill cancer cells and induce the inflammatory reaction. But the

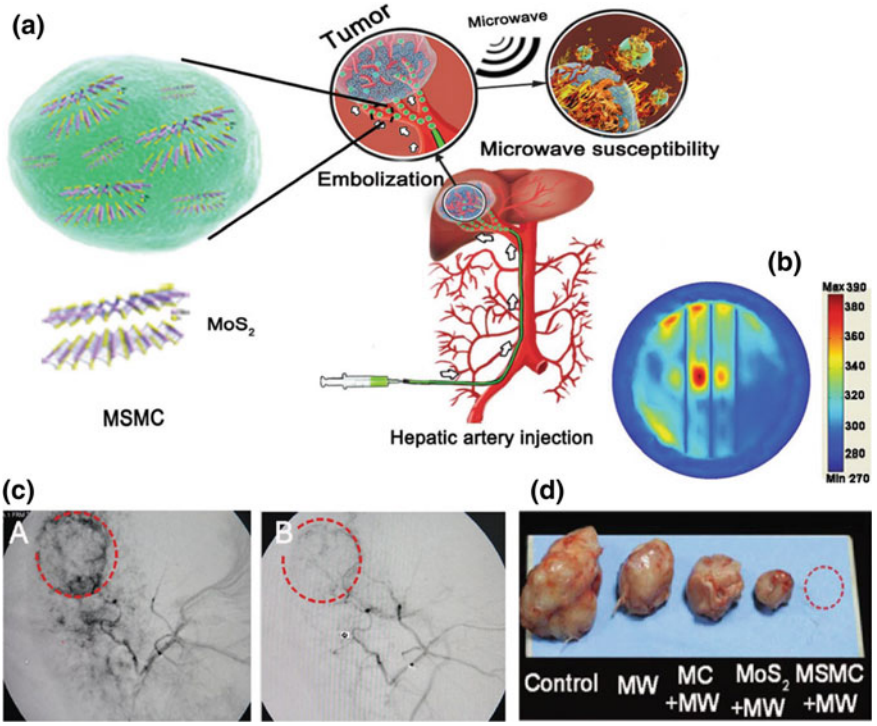

Fig. 8.5 TMDs-based microwave thermal therapy. **a** Schematic illustration of the MSMC used for the microwave ablation and the chemoembolization therapy. **b** The simulated microwave susceptibility for MSMC under the microwave irradiation. **c** Digital subtraction angiography images of the liver before and after embolization of MSMC. **d** Tumor tissues removed from the mice. (Adapted from Ref. [151]. Copyright 2017, The Royal Society of Chemistry.)

efficacy of PDT is hindered by the tissue penetration depth of external light, the insufficient water-solubility of PSs, the targeting delivery of PSs, and the efficiency of ROS generation. For example, the hypoxic tumor microenvironments attenuate the production of singlet oxygen in a photodynamic process and hence reduce therapeutic efficacy. The combination of PTT with PDT may be a novel and feasible strategy to tackle the problems. PTT-caused hyperthermia may soften microvasculature and then increase intratumoral blood flow, which further transports more oxygen into the tumor to improve PDT efficiency [25, 90].

2D TMDs, as a kind of excellent photothermal agent, possess great promising for the combination of PTT and PDT. For example, 2D TMDs have large surface areas, which endow them as photosensitizer carriers to load and delivery molecular PSs. In addition, 2D TMDs-mediated PTT can enhance PDT efficiency by increasing intratumoral oxygen concentrations as well as by promoting the cellular delivery of PSs. Moreover, TMDs own the tunable size and optical properties, which endue them with unique photosensitive behaviors. It is reported that the ultrasonic-exfoliated MoS_2

nanodots can produce massive toxic $^1O_2$ upon a light irradiation [39, 54, 153], even higher than commercial photosensitizer PpIX [154]. BSA-coated MoS_2 nanosheets have also been found to be a photosensitizer for the in vivo NIR light (808 nm) triggered photodynamic cancer treatment [54]. Most importantly, the combination of PTT and PDT can promote the cancer killing efficiency in a synergistic manner.

Yong et al. [87] pioneered the utilization of TMDs for PTT/PDT combined therapy. Water-soluble BSA modified WS_2 nanosheets were prepared by a H_2SO_4 exfoliation strategy. Methylene blue (MB) molecules, a common photosensitizer, were then loaded onto the surface of the as-prepared BSA-WS_2. The greatest HeLa cell prohibition was observed when incubated with BSA-WS_2@MB and exposed to an 808 nm laser (1 W/cm^2, 15 min) and then a 665 nm LED lamp (50 mW/cm^2, 5 min). MB could efficiently product singlet oxygen under irradiation in a controllable manner. The synergistic effects may be ascribed to WS_2-based PTT and MB-based PDT. Not long after, the first 2D TMD-based PDT/PTT combined therapy in the animal model was reported by Liu et al. [61]. The chlorin e6 (Ce6) was selected as the photosensitizer and physically adsorbed onto the surface of MoS_2 nanosheets. The as-prepared MoS_2-PEG/Ce6 nanocomposites could remarkably increase the intracellular uptake of Ce6 molecules because mild hyperthermia could increase cell membrane permeability. The cancer cell growth was significantly inhibited upon the separate exposure of laser with wavelengths at 808 nm (0.45 W/cm^2, 20 min) and 660 nm (5 W/cm^2, 20 min). In similar works, MB-loaded WSe_2-BSA complexes (Fig. 8.6) and PEG-MoS_2-Au-Ce6 nanocomposites also demonstrated to be the promising therapeutic agent for the combination of phototherapy [90, 106].

To increase the release of photosensitizers, a pH-sensitive charge-convertible peptide [LA-K11(DMA)] was modified on the surface of MoS_2 nanosheets and subsequently loading a positively charged photosensitizer (toluidine blue O, TBO) [155]. Under acidic conditions (e.g., tumor microenvironment), the negatively charged LA-K11(DMA) peptide was converted into a positively charged one, reducing the interaction between TBO and MoS_2. Moreover, light-induced hyperthermia could promote the release of TBO, leading to a synergistic tumor therapy. In addition, the promotion of the targeting ability of photosensitizers is also of great importance for PDT [156, 157]. Herein, folic acid (FA) was selected to be decorated on the surface of MoS_2-UCNPs to form a tumor-targeting nanocomposite [157]. To study the target specificity of the as-prepared MoS_2-UCNPs-FA/ZnPc, two types of FR-positive cells and one type of FR-negative cell were incubated with MoS_2-UCNPs/ZnPc or MoS_2-UCNPs-FA/ZnPc, respectively [157]. Strong ZnPc fluorescence was observed in the group of FR-positive cells incubated with MoS_2-UCNPs-FA/ZnPc, while FR-positive cells incubated with MoS_2-UCNPs/ZnPc, and all FR-negative cells emitted negligible ZnPc red fluorescence. These results accelerated the application of 2D TMDs-based nanoplatforms in phototherapy.

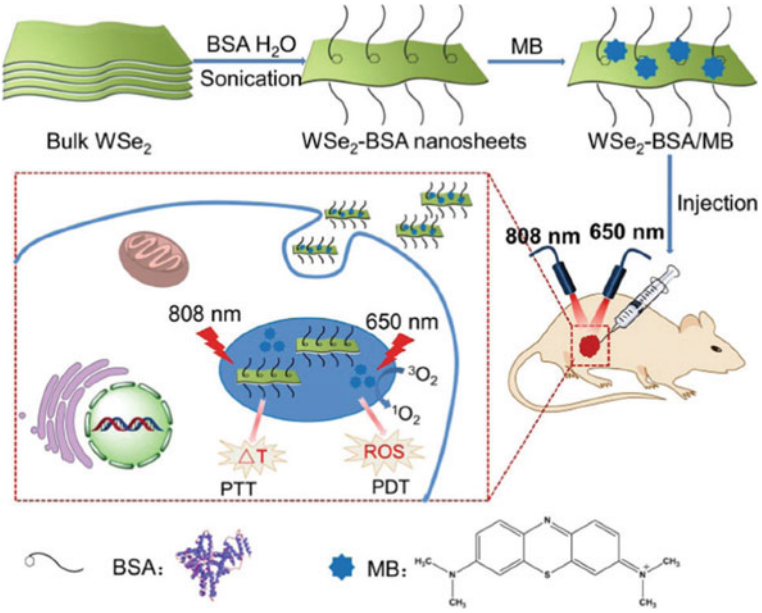

Fig. 8.6 TMDs-based photodynamic therapy. Schematic illustration of the MB-loaded WSe_2-BSA nanosheets for combined PTT/PDT therapy. (Reprinted from Ref. [106]. Copyright 2017, The Royal Society of Chemistry.)

8.5.4 Chemotherapy

Chemotherapy, which utilizes chemotherapeutic drugs for the inhibition and damage of cancer cells, is one of the widely used antitumor approaches in clinical [25]. However, chemotherapy or drugs also meet some shortcomings, such as drug resistance, drug efflux, short circulation time, low specificity or selectivity, insufficient drug-controlled release nanocarriers.

Recent years, 2D TMDs nanomaterials have been demonstrated to be an efficient promoter of chemotherapy. Firstly, TMDs with an ultrahigh surface area and versatile surface chemistry will enable them to feasibly link and delivery drugs. Then, TMDs, as an excellent photo-absorb agent, could trigger the smart drug release at the desired site and time in an external light-controlled manner. In addition, hyperthermia can improve the sensitivity of cancer cells to drugs and increase the drug uptake and accumulation. Moreover, the combination of PTT and chemotherapy can obtain an enhanced synergistic antitumor effect. Therefore, it is necessary to develop the novel and smart NIR light-responsive drug-controlled release systems for chemotherapy.

In the last decade, various NIR light and pH-responsive drug-controlled release systems based on 2D TMDs have been successfully developed [53, 82, 89, 92, 94, 96, 103, 105, 107, 141, 158–163]. For example, as shown in Fig. 8.7, Yin et al. [92] employed CS@MoS_2 as DOX carriers to construct a NIR light-triggered drug

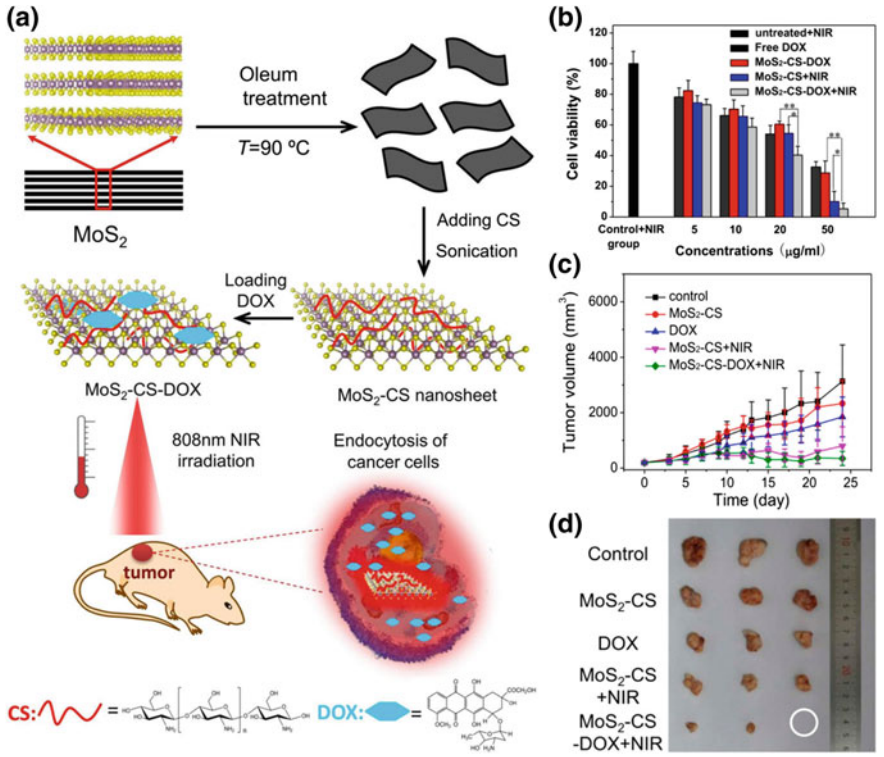

Fig. 8.7 TMDs-based Chemo/PTT combination therapy. **a** Schematic illustration of the CS@MoS_2-based photothermal-triggered drug delivery system for efficient cancer therapy. **b** Cytotoxicity of KB cells treated with CS@MoS_2 with or without irradiation. **c**, **d** The antitumor efficacy of synergistic Chemo/PTT therapy. (Reproduced with permission from Ref. [92]. Copyright 2014, American Chemical Society.)

release system for effective cancer treatment. The DOX loading data showed that the saturated loading rate of CS@MoS_2 was up to ~32% at pH 8.00. In the presence of 808 nm laser irradiations (0.8 W/cm^2, 10 min), 12.4% DOX was released within 1 h in PBS buffer (pH 5.00); while only ~6% DOX was measured without irradiation. This feature will be beneficial to the release of DOX in the acidic tumor microenvironments under external irradiation. In addition, only 0.2% of DOX was released in the next hour in the absence of laser. The accumulated release of DOX was up to 38%, while 80% of DOX was released when the laser power increases to 1.4 W/cm^2. It means that the release of DOX was in a pH and light-controlled manner.

In a similar work, PEG-TaS_2-DOX could also realize the controlled drug releases triggered by NIR light, and moderate acidic pH, leading to the accumulation of drugs [89]. After arriving at the mild acidic tumor microenvironment, those nanoplatforms could effectively release the chemotherapeutic drugs and synergistically damage the cancer cells under the irradiation of external NIR laser.

To realize the slow release of drug and reduce its systemically side effects, Wang et al. [65, 66, 164] designed a series of injectable MoS_2 and drug co-encapsulated implant for NIR light-triggered synergistic PTT and chemotherapy. For example, they fabricated a PLGA/MoS_2/DOX (PMD) oleosol by homogenizing Poly(lactic-*co*-glycolic acid) (PLGA), MoS_2, and DOX together into *N*-methylpyrrolidone (NMP) [164]. The release of encapsulated DOX was relatively slow at pH 7.4 as well as at acidic pH condition (pH 5.4) due to the shielding effect of hydrophobic of PLGA. However, in an acidic solution, the DOX release rate was increased from 8.7 to 31.8% in the light-treated group [164]. Moreover, the PMD hydrogel could restrain their access to body fluid circulation. Such a pH/light dual-stimuli-responsive drug release implant significantly enhanced cancer therapeutic efficacy and mitigated the side effects on normal tissues.

In addition, the chemotherapeutic effects are often reduced by low specific delivery. To address this problem, Liu's group designed a novel targeting approaches based on MoS_2-mediated disulfide chemistry for drug-targeted chemotherapy [165–167]. The copolymer P(OEGA)-*b*-P(VBA-*co*-KH570) (POVK) was modified on the surface of MoS_2 nanosheets and subsequently loaded with DOX [165]. Then, thiol-functionalized transferrin (Tf-SH) was selected as the targeting ligand and anchored onto the surface of MoS_2 through disulfide bonds (–S–S), which could be easily cleaved in the presence of the reductive intracellular GSH. The as-prepared DOX-POVK-MoS_2-Tf nanocomposites showed good stability in physiological condition but rapidly release DOX upon the synergistic trigger of GSH and acidic conditions. The excellent in vitro antitumor outcomes demonstrated that the transferrin-decorated MoS_2-enabled nanocarriers are promising for targeting chemo-photothermal therapy.

8.5.5 Immunotherapy

Activating the body's own immune system for targeting and eradicating cancer cells has long been a goal in immunology [168]. After decades of development, cancer immunotherapy comes of age and has been regarded as the fourth most important cancer therapy modality, after surgery, radiation therapy, and chemotherapy [168, 169]. As an emerging tumor treatment strategy, cancer immunotherapy offers advantages to patients that include higher overall response rates, promoted durable antitumor responses, reduced metastasis, recurrence, decreased side effects, and better tolerance for some special patients more than traditional treatments [169, 170].

Nano-delivery systems hold great potential for further improving the efficiency of cancer immunotherapy due to their versatile physiochemical properties and advantages in efficient tissue-specific delivery, enhanced tumor microenvironment responsiveness [170]. Various types of nanovehicles (e.g., inorganics [171], nanoscale metal-organic frameworks (nMOFs) [172–174], polymers [175], liposomes [176], DNA hybrid [177]) have been studied for anti-metastatic cancer immunotherapy. But up to now, the TMDs-based immunomodulators are relatively scarce. Pardo et al.

[178] reported that WS_2 nanotubes (INT-WS_2) and inorganic fullerene-like MoS_2 (IF-MoS_2) nanoparticles could induce low levels of the proinflammatory cytokines IL-1β, IL-6, IL-8, and TNF-α in human bronchial cells and activate the antioxidant response. Owing to the excellent photothermal performance and delivering capability of TMDs, Han and Wang et al. [104] found that cytosine-phosphate-guanine (CpG) and PEG-functionalized MoS_2-PEG-CpG nanoconjugates could disturb the proliferative activity of 4T1 cells upon NIR irradiation (808 nm, 2 W/cm^2, 10 min), realizing in vitro photothermal-enhanced cancer immunotherapy. The negatively charged CpG was hard to cross the cell membrane and could be easily biodegraded by nucleases, making it difficult to cross the cell membrane [104]. Fortunately, MoS_2 nanocarriers can efficiently promote the intracellular accumulation of CpG and then increase DC (dendritic cells) maturation and TNFα generation, and finally improve the immune response level. The results demonstrated that TMDs-based NIR light-responsive nanovehicles could specifically eradicate tumor-associated immune cells or induced an inflammatory immune response by activating killer T cells [179]. Those preliminary studies will stimulate the development of nanomaterial-based photo-triggered cancer immunotherapy.

8.5.6 Radiotherapy

Radiotherapy or radiation therapy (RT), as an important procedure for many types of cancer, employs ionizing radiation to kill cancer cells [25, 180]. The high energy ionizing radiations in radiotherapy can directly damage intracellular DNA to cause its structural and functional changes and simultaneously indirectly break DNA by the free radicals. In the indirect process, the water and biomolecules are dissociated by ionizing radiation to generate toxic-free radicals including ROS. However, RT also has some drawbacks, such as the requirement of elevated doses, the side effects to normal tissue, and the radioresistance of hypoxic cancer cells [29, 180].

With the development of emerging nanomedicine, two feasible approaches come into being to enhance the efficiency of RT [25]. Since the high Z element possesses strong X-ray attenuation ability, the first strategy is to improve the effectiveness of external ionizing radiation by using nanoradiosensitizers which contain elements with high atomic number (e.g., Au, Gd, Hf, Ta, W, Bi) [29]. The high Z element could increase energy deposition and then generate secondary and Auger electrons, which can efficiently cause DNA damages and suppress cell growth [72, 77, 100]. The other is to modulate tumor microenvironment (e.g., hypoxia, H_2O_2, low pH) or disturb cellular biochemical process (e.g., cell cycle, DNA repair) by using multifunctional nanoparticles [29, 181]. For example, hyperthermia not only can directly kill cancer cells but also inhibit the repair of damaged DNA by inducing protein aggregation [146]. In addition, as mentioned above, hyperthermia can increase intratumoral blood flow, which may relieve the hypoxic microenvironment, making cancer cells more susceptible to radiation [146]. Moreover, hyperthermia can damage the cancer cells

which are resistant to ionizing radiation. Hence, the combination of PTT and RT may be a feasible approach to improve the therapeutic effects of RT alone.

Some TMDs (e.g., MoS_2 [68], WS_2 [72, 86, 88, 97, 100], ReS_2 [77]) with strong X-ray attenuation ability have the potential for facilitating the combination of PTT and RT into one system. For example, Yong et al. [86] designed biocompatible WS_2-PEG with ultrasmall size (3 nm) via a facile H_2SO_4 exfoliation strategy. The as-prepared WS_2-PEG possesses good water-solubility, low cytotoxicity, high absorbance in the NIR region, and more importantly, strong X-ray attenuation performance. After the treatment of NIR light plus X-ray radiation, the remarkable DNA breaking was observed in the group of 4T1 cells incubated with WS_2-PEG, as shown in Fig. 8.8. Encouraged by the excellent outcomes of in vitro experiment, the tumor-bearing mice were i.t. injected with WS_2-PEG solutions and then treated with PTT and RT separately. Three weeks later, tumor growth in the treated group was significantly delayed. In addition, the Liu group also reported the use of PEGylated WS_2 nanocomposites (e.g., Gd^{3+}-doped WS_2-PEG [72], MnO_2 coated $WS_2@Fe_3O_4/sSiO_2$ [97]) as multifunctional agents for RT involved combination cancer therapy. In those works, W and Gd atoms strongly deposit X-ray energy to promote the generation of toxic ROS for radiosensitization. Besides, the catalytic MnO_2 with pH-responsive ability can decompose tumor endogenous H_2O_2 and relieve tumor hypoxia to further reverse the radioresistance of hypoxic cancer cells. WS_2-mediated PTT could also effectively kill the radioresistant cancer cells, leading to the remarkably PTT-enhanced RT therapeutic effects. Differ from external-beam radiation therapy, radioisotope ions labeled WS_2-PEG (^{188}Re-WS_2-PEG) could realize "self-sensitization" to enhance the synergistic effects of PTT and internal radioisotope therapy without the demand of external X-ray source [100]. After the treatment, the tumors were gradually eradicated and the mice survived for more than 60 days.

8.5.7 Radioprotection

Although radiotherapy is a widely used and highly effective treatment for cancer therapy, it also causes inevitable damage to healthy tissues in the body. Radioprotection, which makes use of radioprotectants to protect healthy tissues from radiation damage, is becoming increasingly important [182, 183]. There is an urgent demand for designing highly efficient radioprotectants to relieve the pain of patients.

Ionizing radiation can directly damage cellular DNA and indirectly damage DNA by the generation of cytotoxic free radicals. On this account, the strategy of radioprotective often originates from the scavenging of free radicals. Different from radiosensitizers, which aim to improve the generation of free radicals in tumor tissues, radioprotectors provide a feasible approach to shield healthy tissues from radiation damage. The most remarkable radioprotectors are the sulfhydryl (SH) compounds, such as cysteine and cysteamine, which could protect animals from total body exposure to irradiation [184]. Amifostine, which is the first selective-target and broad-spectrum radioprotector [184, 185], has been used as a protector for radiotherapy as well as

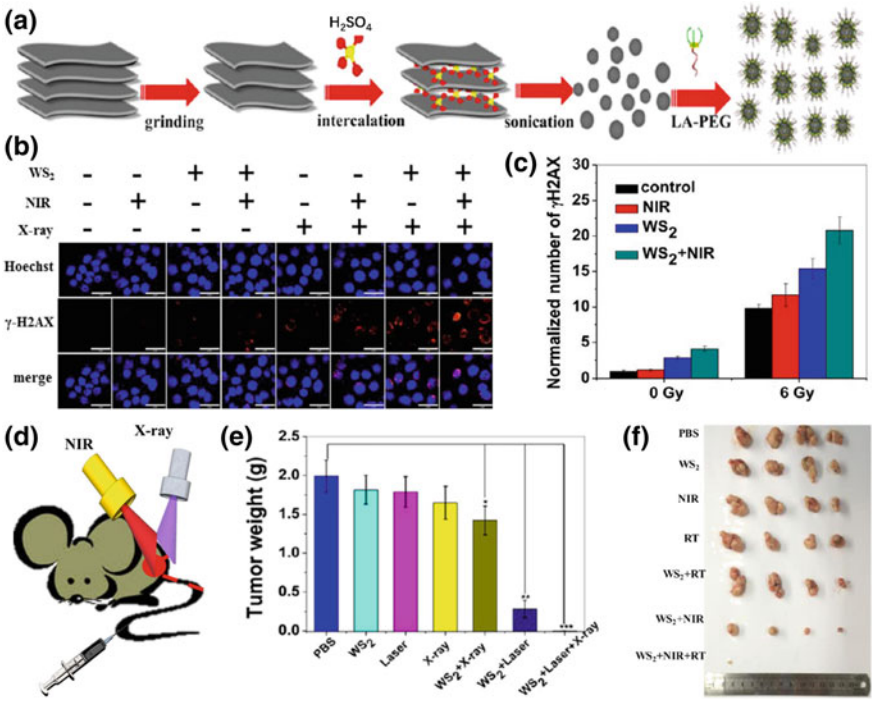

Fig. 8.8 TMDs-based PTT/RT combination therapy. **a** Synthetic process diagram of WS_2 QDs. **b** Representative fluorescence images of DNA fragmentation and nuclear condensation induced by WS_2 QDs and external NIR laser and X-ray treatment. **c** Corresponding normalized number of γ-H2AX after WS_2 QDs and external NIR laser and X-ray treatment. **d** Scheme of the WS_2 QDs-based PTT/RT combined therapy. **e**, **f** The antitumor efficacy of combined PTT/RT therapy. (Reproduced with permission from Ref. [86]. Copyright 2015, American Chemical Society.)

chemotherapy due to its quick accumulation in normal tissues and little penetration into tumors [184]. But the side effects and short blood circulation half-life [186] of amifostine seriously impede its extensive uses. Therefore, it is of great importance to developing more ideal radioprotectors to address these critical challenges.

The emerging nanobiotechnology provides such an opportunity for developing alternative radioprotectors [183]. Ceria (CeO_2) nanoparticles are one of the most representative nanoradioprotectors revealed to show remarkable free radical scavenging performance and radioprotection effects in vivo and in vitro [187–190]. In addition, some carbon nanomaterials (e.g., bamboo charcoal [191], multiwalled carbon nanotubes [192], graphene [193], graphdiyne [182]) also have free radical scavenging ability for radioprotection. Yim et al. [194] deeply studied the ROS scavenging mechanisms in vitro of TMDs nanosheets based on experimentally ROS detections and theoretically simulations. They thought that the radical-mediated oxidation of TMDs and hydrogen transfer from the oxidized TMDs to radicals were the two main steps involving ROS scavenging. Recently, the Zhang group pioneered the study of

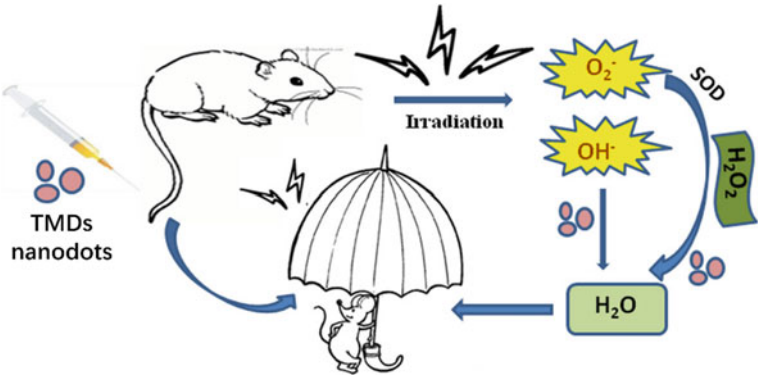

Fig. 8.9 TMDs-based radioprotection. Schematic illustration of the radioprotective process of the ultrasmall MoS_2, WS_2, and WSe_2 nanodots. (Reproduced with permission from Ref. [196]. Copyright 2017, American Chemical Society.)

TMDs-based radioprotectors for radioprotection in vivo [195–197]. For example, they designed ultrasmall cysteine-protected MoS_2 dots with high catalytic properties as radioprotectants. The electrochemical measurements showed that the as-prepared cysteine-protected MoS_2 dots exhibit strong in vitro catalytic activities for H_2O_2 and oxygen reduction reactions. The catalytic capability of the ultrasmall MoS_2 dots might stem from its size effect and surface atomic defects. The A31 cells were incubated with cysteine-MoS_2 dots in different concentrations and then exposed to various gamma radiation doses. At the same doses of radiations, the survival rates of cells were significantly increased with increasing cysteine-MoS_2 concentrations, suggesting an efficient protective phenomenon against external radiation damages in vitro. The tail moment experiments showed effectively DNA repair in the cysteine-MoS_2 dots-treated group. The reason is that the catalytic properties enable MoS_2 dots to scavenge free radicals via rapid reactions with $\cdot O_2^-$ and H_2O_2 and thus reduce DNA damage. It is well known that radiation can destroy healthy cells in the body, especially bone marrow cells and cells in the gastrointestinal tract [198]. So, we can assess the level of in vivo radioprotection by analyzing the DNA concentrations of bone marrow cells. After 7 days post-exposure to radiation, the total DNA in bone marrow cells and bone marrow nucleated cells recovered to the health level in the MoS_2-treated group, resulting in the enhanced surviving fraction of mice. It is worth to note that cysteine with SH group also can scavenge free radical and repair DNA, which is mentioned above. But the author observed only a low survival rate of cysteine-treated mice, clearly indicating that the principal radioprotection effects originated from MoS_2 instead of cysteine. Similarly, they also developed highly catalytic ultrasmall (sub-5 nm) cysteine-protected WS_2 [196] and WSe_2 [197] dots with renal clearance to scavenge free radicals for radioprotection (Fig. 8.9).

8.5.8 Combination Therapy

The current trend in nanomedicine has gradually shifted from monotherapy to combination therapy for enhanced treatment efficacy [199]. In Table 8.1, we can conclude that significant progress has been achieved in 2D TMDs nanomaterials-mediated multimodal combination therapy in the recent decade. Since their multifunctional physicochemical properties, such as high surface area, versatile surface chemistry, excellent photothermal conversion efficacy, and strong X-ray attenuation ability, 2D TMDs can be designed on demand for the combination of diagnostic applications (e.g., FL, PAT, CT) and therapeutic applications including PTT, MWT, PDT, chemotherapy, and RT. The combined therapy can not only overcome the shortcoming of monotherapy but also may obtain the remarkable superadditive (namely "1 + 1 > 2") effects in the battle against cancer.

8.6 Tissue Engineering

Tissue engineering aims to develop biological substitutes that restore, maintain, or improve damaged tissue and organ functionality [200]. During the past ten years, multifunctional nanomaterials have been served as alternative biomaterials to traditional implants and recognized as promising candidates for bone, vascular, neural, and bladder tissue engineering applications.

As a new type of inorganic biomaterials analogous to graphene, TMDs not only attract extensively interest in bioimaging and cancer therapy but also show great potentials for tissue engineering although research works in this field are only at a beginning stage. On the one hand, TMDs with versatile physicochemical properties can act as reinforcing agents within biopolymers. Due to the high Young's modulus and functional group, WS_2 nanotubes have been utilized to increase and reinforce the mechanical properties of biodegradable poly(propylene fumarate), which is widely investigated for bone tissue engineering [201]. In addition, the atomic defects of 2D MoS_2 (mostly due to sulfur vacancies) can offer a facile binding center for four-arm poly(ethylene glycol)-thiol (PEG-SH) via covalent conjugation, forming a high-water content gel [202]. The hydrogel obtained from vacancy-driven gelation exhibits better cytocompatibility and elastomeric and robust mechanical behavior. On the other hand, TMDs reinforced nanofibers or scaffolds with excellent biocompatibility and various fascinating properties can be applied to tissue engineering, especially stem cells proliferation and bone regeneration. It is well known that electrospinning is a simple yet effective approach to fabricate ECM-like nanofibrous materials with desirable performances for tissue engineering [203]. For example, prepared by electrospinning technology, as shown in Fig. 8.10, the polyacrylonitrile/MoS_2 composite nanofibers showed low cytotoxicity and natural ECM-like structure [203]. Moreover, they could guide effective adhesion and differentiation of bone marrow mesenchymal stem cells (BMSCs) on nanofibers. This phenomenon indicated that the as-prepared

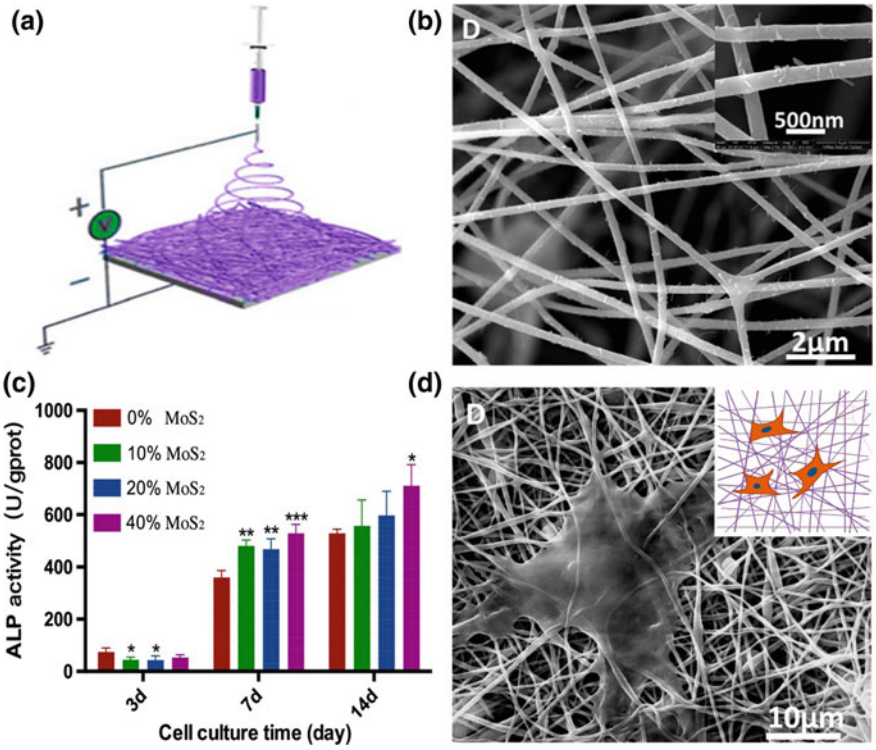

Fig. 8.10 The use of TMDs for tissue regeneration. **a** Schematic illustration of the fabrication of MoS_2 composite nanofibers by electrospinning technology. **b** SEM images of MoS_2 composite nanofibers with 40% MoS_2 (w/w). **c** Alkaline Phosphatase activity of BMSCs cultured on different MoS_2 composite nanofibers in various incubation periods. **d** SEM images of BMSCs cultured on 20% MoS_2 composite nanofibers on day 3. (Reproduced with permission from Ref. [203]. Copyright 2017, American Chemical Society.)

MoS_2 nanofibers could promote the growth of stem cells and positively regulate cellular proliferation and osteogenic differentiation. Similarly, nanostructured MoS_2 also has the potential to promote the differentiation of neural stem cell (NSC) and the maturation of neurons.

Wang et al. [22] designed nanostructured MoS_2 thin films (MTFs) on glass slides via a bottom-up hydrothermal process. When seeded and cultured NSCs on an MTF, they found that biocompatible MTFs played important roles in promoting cell attachment on films and directing NSC differentiation. Motivated by their comparable performance than tissue culture plate, these MoS_2 thin films were then used to assemble with an electrospun PVDF support substrate matrix to construct 3D living conduit scaffolds for nerve regeneration. 3D bioprinting is another emerging popular technique to fabricate extracellular matrix biomaterials for tissue engineering including bone regeneration in recent decades [204]. For example, Wang et al. [23] for the

first time reported a bifunctional 3D-printed bioceramic scaffold for simultaneous tumor therapy and tissue regeneration. The as-fabricated porous scaffold with good biocompatibility comprised two functional parts: akermanite ($Ca_2MgSi_2O_7$) as the matrix material for osteogenesis and angiogenesis, and MoS_2 nanosheets as photothermal agent for NIR tumor ablation. After implanting the hybrid scaffolds into the center of tumors and then exposed to an 808 nm laser, the temperature in tumor tissue rapidly increased to ~50 °C. Moreover, akermanite contained scaffolds could contribute to the attachment, proliferation, and osteogenic differentiation of BMSCs and promote bone regeneration in the rabbit model, indicating that the scaffolds have the potential to act as bioactive materials for bone regeneration. This studies provide a promising strategy to overcome tumor-induced bone defects and opens a new way for the combination of tumor therapy and tissue engineering by using TMDs-based multifunctional inorganic nanomaterials.

8.7 Medical Devices

Since TMDs possess versatile promising physicochemical properties, such as electrical, mechanical, and catalytic property, it has attracted significant attention particularly in biomedical devices for many types of diseases.

Medical strips, such as woundplast, are the most commonly used external medication. Strips usually consist of rubberized fabric and infused therapeutic drugs for hemostasis, wound antibiosis and skin infection, and so on. Recently, nanotechnology has shown the potentials to revolutionize traditional medical strips. For example, some nanomaterials with enzymatic property (e.g., peroxidase) have been successfully used to fabricate strips for effective and sensitive detecting H1N1 virus [205]. Cao et al. [20] infused the cysteine-MoS_2 with Ag^+ ions and then coated with a layer of cationic polyelectrolyte to fabricate an antibacterial depot for wound disinfection in vivo (Fig. 8.11). The biocompatible MoS_2 nanosheets not only possess antibacterial ability [21] but also can efficiently adsorb Ag^+ and then release it to the cell walls. Inspired by Cao's work [20], $MoSe_2$ hybrid nanosheets were twined by silk fibroin to form macroscopic films [46] (Fig. 8.11). Then, the films were posted on the *E. coli* infected skin wounds on the mice. Due to the superior peroxidase-like activity, $MoSe_2$ nanosheets can catalyze the decomposition of H_2O_2 into ·OH radicals, which possess high antibacterial ability without bacterial resistance. Therefore, a rapid and effective wound disinfection and healing efficacy were observed after treating with silk fibroin-coated $MoSe_2$ films and low-dose H_2O_2 in vivo. Those proof-of-concept studies demonstrated the feasibility of wound disinfection in wound care management using catalytic TMDs-based medical strips [20, 21, 46].

Soft bioelectronics, employing soft materials whose modulus is well matched with soft human tissues, have been extensively used in internal environment owing to their soft mechanical properties that lead to minimize tissue damages and immune responses [24]. For instance, there is still a challenge to fabricate implantable artificial retina simultaneously with the function of optoelectronic sensing and retinal stimu-

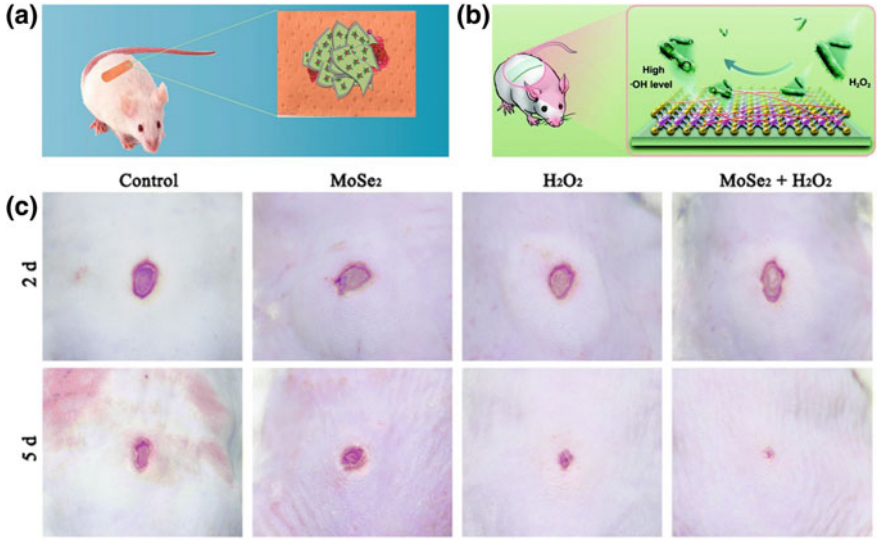

Fig. 8.11 TMDs-based woundplast for wound disinfection. **a**, **b** Schematic illustration of the preparation TMDs-based woundplast (Reprinted with permission from Ref. [20]. Copyright 2017, American Chemical Society.) **c** The wound repair process on the mice by the use of the silk fibroin-$MoSe_2$ films (Adapted from Ref. [46]. Copyright 2017, The Royal Society of Chemistry.)

lation. Therefore, Choi and his co-workers [24] designed an ultrasoft, high-density and hemispherically curved image sensor (CurvIS) array based on the atomically thin MoS_2-graphene heterostructure, as shown in Fig. 8.12. The soft, ultrathin, as well as super photo-absorption coefficient enables MoS_2 nanosheets as a photodetector to achieve high-quality imaging, while the ultrathin graphene acts as electrodes to conduct photocurrent. The CurvIS array exhibits many advantages including the high-density array design, hemispherical shape, small optical aberration, and simplified optics. It was found that the soft MoS_2-graphene CurvIS array successfully stimulated a rat's retinal nerves in response to the pulsed external optical signals. This deep work might greatly promote the application of 2D ultrathin nanomaterials-based implantable soft bio-optoelectronic device in ophthalmology.

8.8 Toxicity and Biosafety

8.8.1 Nanotoxicity Mechanisms of TMDs

The clinical translation of nanomaterials and nanotechnology gives rise to the high awareness of nanotoxicity and nanosafety originated from the public and scientific community. The toxicity of TMDs is of great importance and should be first con-

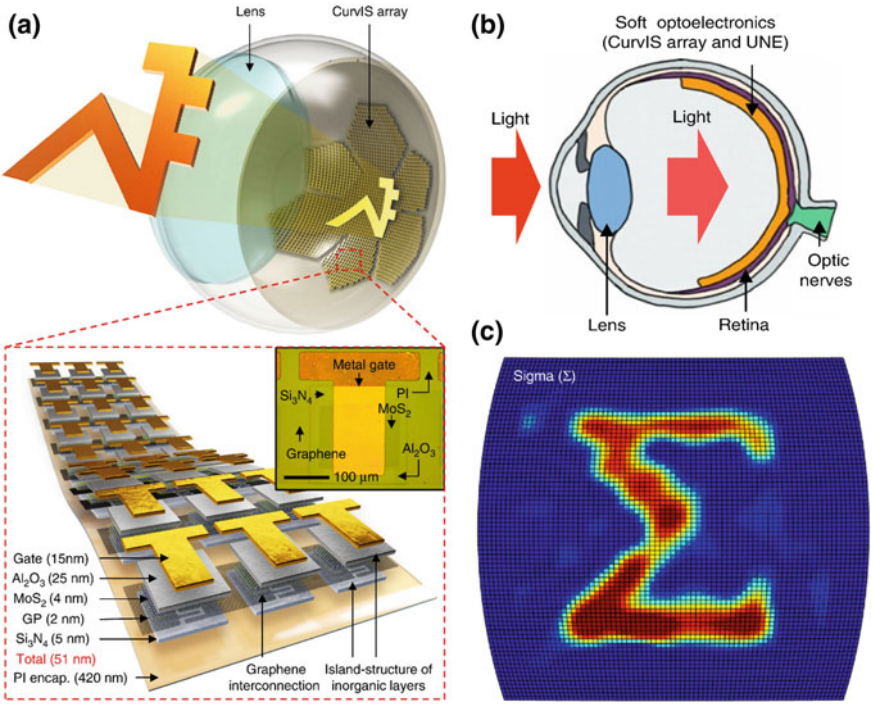

Fig. 8.12 TMDs-based soft bioelectronics for ophthalmology. **a** Schematic illustration of the high-density CurvIS array based on the MoS_2-graphene heterostructure. **b** Schematic illustration showing the ocular structure with the soft optoelectronic device. **c** Sigma-shaped image captured by the CurvIS array (Reproduced with permission from Ref. [24]. Copyright 2017, Springer Nature.)

sidered to guarantee their safe uses in the biomedical field. Therefore, since TMDs have shown great promising in disease diagnostic, bioimaging and cancer therapy, we are bound to pay more attention to study their biological effects and toxicology profiles in vitro and in vivo.

The interaction of 2D TMDs nanosheets with biosystems plays a vital role in understanding the nanotoxicity mechanisms of TMDs and guiding their safe and biomedical application. A deep study on cellular-level revealed the nano-bio interactions of MoS_2 nanosheets (the representative example of 2D TMDs family) with cancer cells from the aspect of endocytosis/exocytosis and autophagy [206]. As shown in Fig. 8.13, the main internalization processes and intracellular tracks of MoS_2 nanosheets consist of three different pathways: endocytosis through macropinocytosis, transportation from early endosomes to lysosomes, secretion of the internalized MoS_2 via exocytosis. Moreover, autophagy is also involved in the accumulation of MoS_2 in the lysosomes. So far, as the Achilles' heel, the biosafety evaluation and toxicity mechanisms of different types of TMDs in the biosystems are still not well revealed and understood [207].

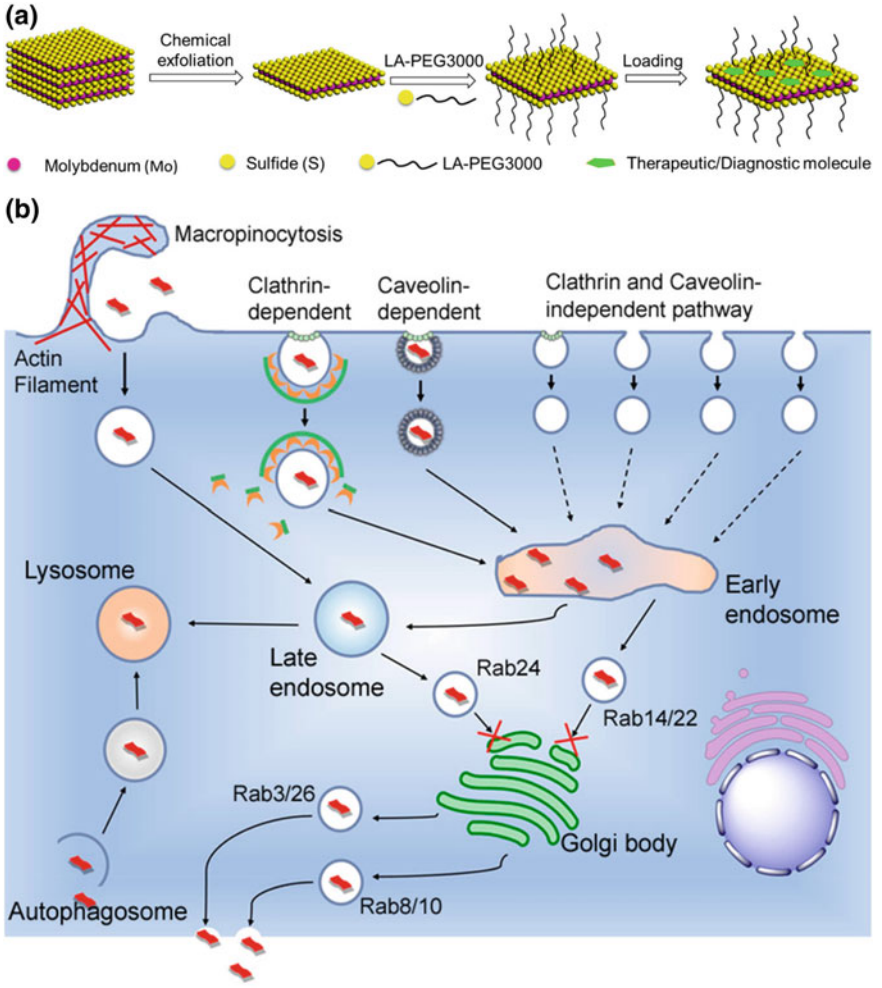

Fig. 8.13 The nano-bio interactions of MoS_2 nanosheets with cancer cells. **a** Scheme of the preparation of MoS_2 nanosheets with therapeutic/diagnostic molecules. **b** Schematic diagram illustrating the intracellular fates of MoS_2-based nanosheets. The process consists of three different pathways: endocytosis through macropinocytosis, transportation from early endosomes to lysosomes, secretion of the internalized MoS_2 via exocytosis. (Reproduced with permission from Ref. [206]. Copyright 2018, American Chemical Society.)

On the one hand, when TMDs nanoparticles enter the body, it may cause many stress reactions such as ROS production as it can be regarded as foreign components by cells and tissues. ROS usually generated from different routes such as the direct production, the interaction with cellular organelles, and the catalysis of intracellular H_2O_2 and so on. However, various negative effects, especially cell apoptosis or necrosis, will be appeared when the ROS level is too high. So, we must find out the safe concentrations and permissible doses of TMDs to ensure the minimum harmfulness to healthy tissues. It is worth mentioning that the generation of ROS caused by TMDs is an effective strategy to prohibit the growth of bacteria and cancer cells for antibacterial and antitumor, respectively. On the other hand, TMDs can be gradually biodegraded by various degradative components or the physiological environment, resulting in the release of free metal ions from TMDs, which may be also contributed to the toxicology profiles. For example, similar to CdS nanoparticles, Shang et al. demonstrated that the antibacterial activity of WS_2 was not only caused by ROS generation but also related to the release of toxic tungsten ions under UV irradiation [39]. Besides, the outstanding physicochemical properties such as the large surface area, surface atomic vacancy, and surface charge enabled TMDs nanosheets to interact with surrounding biological molecules via electrostatic interaction, covalent conjugation, or van de Waals forces. For example, the interaction of MoS_2 with protein can be investigated by all-atom molecular dynamics simulations [208–210]. The simulation results show that the secondary and tertiary structures of β-sheet protein were quickly damaged after adsorbing onto the MoS_2 surface [208]. In a later work, Villin Headpiece (HP35), a model protein widely used in protein folding studies, was chosen to further study the potential toxicity of MoS_2 nanosheets to proteins at the atomic level. MoS_2 nanosheets exhibit robust denaturing capability to severely destroy the secondary structures of HP35 within hundreds of nanoseconds. The dispersion interaction between protein and MoS_2 monolayer is contributed to the main driving force behind the adsorption process. Those interesting works illustrated the nanotoxicology origination from the atomic and theoretical levels, which help us to understand the underlying molecular mechanism. Then, Zou et al. [211] revealed for the first time that single-layer MoS_2 ($SLMoS_2$) accelerated proliferation and promoted myogenic differentiation and epithelial-mesenchymal transition (EMT) in human embryonic lung fibroblasts (HELFs) via the Akt-mTOR-p70S6 K signaling pathway, which is triggered by the generation of ROS. In contrast, after BSA binding, the cellular uptake of $SLMoS_2$ and the production of intracellular ROS were markedly reduced, and the $SLMoS_2$-activated phosphorylation of Akt-dependent signaling pathways was also mitigated. This studies demonstrated that serum proteins binding provides an effective strategy to reduce the potential nanotoxicity of MoS_2 nanosheets. So, after being uptake into tissue, TMDs will be coated by serum proteins, forming a protective protein corona.

8.8.2 *Effects of Physicochemical Factors on Nanotoxicity*

Compared to the corresponding bulk material, TMDs nanosheets have unique properties which can greatly affect the biological interaction of TMDs with cells. According to previous studies, the biocompatibility and nanotoxicity of TMDs nanosheets may vary with different synthesis methods, surface modification, size, shape, number of layers, surface charge, chemical composition, dose as well as the exposure time and route [212, 213]. The mainly physicochemical factors influencing biocompatibility of 2D TMDs nanosheets are as follows.

(1) **Preparation methods**

Chemically exfoliation is a well-known and widely used method to prepare biocompatible 2D TMDs for biosensing and cancer treatment. However, little is known about the degree of exfoliation of the nanosheets impacting on their toxicological behaviors. In one such recent work, Chng et al. [214] systematically compared the toxicity in vitro of MoS_2 nanosheets, which were chemically exfoliated using various lithium intercalating agents. All the results of the methylthiazolyldiphenyltetrazolium bromide (MTT) and water-soluble tetrazolium salt (WST-8) assays on A549 cells indicated that the *tert*-butyllithium (*t*-Bu-Li) and *n*-butyllithium (*n*-Bu-Li) exfoliated MoS_2 nanosheets showed higher cytotoxicity than MoS_2 exfoliated by methyllithium (Me-Li). In fact, the cytotoxicity of Me-Li-exfoliated nanosheets was similar to that of bulk MoS_2. *t*-Bu-Li and *n*-Bu-Li provide more efficient exfoliation over Me-Li, indicating that MoS_2 nanosheets exhibit stronger toxicity with increased exfoliation and decreased layer number. In contrast, a separate work by Wang et al. [215] has reported the increasing toxicological potential of three aqueous suspended forms of MoS_2 with increasing thickness or aggregates. It was observed that the aggregated and layered MoS_2 nanomaterials did not induce significant in vitro cytotoxic effect on BEAS-2B and THP-1 cell lines. Compared to lithiation-exfoliated MoS_2 (Lit-MoS_2) and Pluronic F87-dispersed MoS_2 (PF87-MoS_2), aggregated MoS_2 (Agg-MoS_2) induces stronger in vitro proinflammatory and profibrogenic responses. Moreover, Agg-MoS_2 caused acute lung inflammation in mice model, while both Lit-MoS_2 and PF87-MoS_2 had little effect. The observed phenomenon suggests that exfoliation attenuates the toxicity of Agg-MoS_2. Hence, it is a tremendous need to standardize the preparation of TMDs for toxicity tests.

In addition, the cytotoxicity of 2D TMDs may vary with different preparation methods. For example, Appel et al. [217] carefully investigated the toxicology profiles of mechanically exfoliated and CVD-grown pristine 2D TMDs (ME-WS_2, MEMoS_2, and CVD MoS_2) through various biocompatibility tests, including live-dead cell assays, ROS generation assays, and cellular morphology assessment. It turns out that both mechanically exfoliated and CVD-grown TMDs do not decrease cell viability and induce genetic defects when the concentrations of TMDs as high as 100 μg/mL.

(2) **Surface modification**

Taking MoS_2 as an example, Liu et al. [103] firstly studied the in vitro toxicity of pristine and PEGylated MoS_2 nanosheets using MTT assay. HeLa cells were incubated with various concentrations of MoS_2 or MoS_2-PEG for 24, 48, and 72 h. It was found that pristine MoS_2 nanosheets exhibited slight cytotoxicity (cell viability is ~73%, MoS_2 at 0.16 mg/mL) after culturing for 3 days, while PEGylated MoS_2 nanosheets showed negligible cytotoxicity (cell viability over 90%). The intracellular ROS levels in MoS_2 treated cells were subsequently assessed by using dihydroethidine (DHE) probe, indicating minimal oxidative stress induced by MoS_2. Moreover, PEGylated MoS_2 nanosheets also exhibited no significant cytotoxicity at a series of concentrations up to 500 μg/mL [111]. The novel outcomes of this work may be ascribed to the PEG-mediated one-pot solvothermal procedure. The "bottom-up" strategy improves the colloidal stability and bio-tolerance of MoS_2 nanosheets in the physiological environment. A separate study conducted by Pumera group also revealed that thiobarbituric acid functionalized MoS_2 nanosheets showed more protective effects than non-functionalized MoS_2 [218]. Thereafter, many works have been developed based on biocompatible polymers, liposomes, and even cellular components functionalized approaches to reduce the cytotoxicity of MoS_2 nanosheets. The excellent biocompatibility inspires the researchers to further pursue the biomedical applications of MoS_2.

(3) **Size and morphology**

Nanoparticle size and morphology play important roles when interacting with biological molecules and cells present in physiological conditions. In one such study, three kinds of cells (THP-1, AGS, and A549 cells) were incubated with three sizes (50, 117, and 177 nm) of MoS_2 at varying concentrations for 24 h [219]. The results showed that AGS cells were the most susceptible to 117 nm MoS_2 at the highest concentrations, while THP-1 showed the highest toxicity toward the smallest MoS_2 sheets (50 nm), indicating that the cytotoxicity of MoS_2 nanosheets varies with its sizes and cell types. Besides, some studies reported that the ultrasmall TMDs may be faster and easier to be cleared out of the kidney and body [67, 195–197]. Not only the 2D-layered TMDs nanosheets but other morphological TMDs such as radar-like MoS_2 nanoparticles [123], flowerlike MoS_2 nanoflakes [21, 102, 122, 158], multiwall WS_2 nanotubes [220], fullerene-like nanoparticles (IFWS_2 [220], $MoSe_2$ [221]) also have been demonstrated to be favorable biocompatibility in a certain concentration range.

(4) **Chemical Composition**

The chemical compositions are also key factors impacting on the toxicology profiles of TMDs nanosheets. Pumera group pioneered the study of the nanotoxicity of 2D materials including graphene, black phosphorus, and TMDs. In a work, they found that MoS_2 and WS_2 induced slight cytotoxicity in the A549 cells after 24 h exposure, even at high concentration up to 400 μg/mL, while WSe_2 showed higher toxicity compared to MoS_2 and WS_2 [222]. Moreover, the studied Group 6 TMDs (MoS_2,

WS_2, WSe_2) exhibited significantly lower cytotoxicity than different synthesized graphene oxide (GO) and layered GaSe tested on the same cell lines in the same conditions, while black phosphorus showed a generally intermediate cytotoxicity between GO and TMDs [222–225]. They subsequently compared the toxicological behavior of Group 6 TMDs with Group 5 vanadium dichalcogenides (VS_2, VSe_2, VTe_2) under similar experimental conditions [216]. For the same chalcogen element, VS_2 consistently shows higher toxicity for both MTT and WST-8 assay at all concentrations than that of MoS_2 and WS_2; the similar tendency was also observed among WSe_2 and VSe_2. They also compared the cytotoxicity of the Group 5 transition metal ditellurides (VTe_2, $NbTe_2$, $TaTe_2$) to understand their biological effects for the future applications [226]. The results suggest that VTe_2 is highly toxic to A549 cells with 92.5% of cells elimination at a concentration of 200 μg/mL, whereas $NbTe_2$ and $TaTe_2$ are mildly toxic. For the same metal element, the metal sulfides (WS_2, VS_2) display higher cell viability relative to their corresponding metal selenides (WSe_2, VSe_2) [216]. In addition, a recent work revealed that the toxicity of Pt dichalcogenides follows the trend of $PtTe_2 > PtSe_2 > PtS_2$ [227]. It is concluded that TMDs consist of vanadium element which is inherently more toxic than Mo and W, while sulfides are generally less toxic compared to their selenide and telluride counterparts for TMDs.

8.8.3 Nanotoxicity and Biodegradability of TMDs

To date, many research works have been conducted to evaluate the in vitro cytotoxicity of 2D TMDs through CCK-8, MTT assays, or WST-8 assay. Most of the results showed that 2D TMDs were non-cytotoxic or negligible cytotoxic within a certain range of concentrations, which importantly encouraged the in vivo applications of TMDs. In this regard, researches concerning the evaluations on the biosafety and biodegradability in vivo of 2D TMDs are urgently required. Many studies have reported that the TMDs nanosheets treated mice could survive for more than one month. For example, Liu et al. [103] assessed the biocompatibility of PEGylated MoS_2 nanosheets to BALB/c mice at the dose of 3.4 mg/kg. The results showed that PEGylated MoS_2 nanosheets may not be noticeably toxic to mice within one month. In a similar work, WS_2-PEG (20 mg/kg of i.v. injection) and NIR irradiation (808 nm, 0.8 W/cm^2, 5 min) treated BALB/c mice showed no obvious abnormal behavior and noticeable organ damage within 45 days [59]. The blood biochemistry assay revealed that all measured indexes of the blood test fell within normal reference ranges, indicating the excellent histocompatibility of WS_2-PEG. In addition, 4T1 tumor-bearing mice died within 16 days, while the TiS_2-PEG and PTT treated mice survived over 60 days, suggesting no obvious toxicity to mice at the tested dose [75]. In another in vivo toxicology assays, i.v. injected ReS_2-PEG nanosheets did not induce obvious organ damages, hepatic or kidney disorder at the dose of 20 mg/kg [77]. Besides, Yu et al. [228] conducted the first investigation of the toxicity of CS@MoS_2 micro-sheets in adult zebrafish. It was found that CS@MoS_2 at

high concentrations (20 mg/L) induced a proinflammatory response and apoptosis in the gills and liver.

More importantly, the long-term biodistribution, degradation, and excretion of PEGylated MS_2 (M = Mo, W, Ti) were carefully evaluated and compared by Hao et al. [229]. After i.v. injection, these three kinds of PEGylated TMDs nanosheets were found mainly to be accumulated in liver and spleen. Notably, large amounts of injected W or Ti were still retained in the RES for months, while MoS_2-PEG could be almost completely degraded and then excreted. PEGylated MoS_2 and TiS_2 will be oxidized into water-soluble Mo^{VI}-oxide species (such as MoO_4^{2-}), water-insoluble TiO_2 aggregates, respectively, while WS_2-PEG was hardly oxidized for the higher chemical stability. The histological and blood analysis demonstrated that these three kinds of PEGylated MS_2 nanosheets have no obvious long-term toxicity at the tested dose [229]. In a separate work, ultrasmall VS_2 nanodots converted from their sheet materials via ultrasonic exfoliation exhibited effective body excretion without appreciable toxicity [76]. Dark black VS_2@lipid-PEG solutions were found to be gradually oxidized into light yellow after air exposure 30 days. The results confirmed that V element in VS_2 nanostructures was oxidized from V^{3+}/V^{4+} to the high valence state (V^V). Thus, VS_2@lipid-PEG nanoparticles might be gradually oxidized and degraded into water-soluble and degradable V^V-oxide species.

8.9 Conclusions and Outlook

The utilization of multifunctional TMDs nanosheets for biomedical applications is of great importance and has achieved remarkable advancement. In this chapter, we summarized the latest progress of inorganic 2D TMDs in bioanalysis, antibacterial and wound repair, drug delivery, bioimaging, cancer therapy, tissue engineering, and medical devices. In particular, the nanotoxicology and biosafety profiles of TMDs are reviewed to ensure their further biomedical use. The abundant chemical compositions, unique physicochemical properties, and diverse biological effects endow the emerging TMDs nanosheets with the potential for next-generation biomedicine.

However, the investigation of these 2D TMDs in biomedicine is only in its infancy, and two critical challenges are to be concerned. From the materials point of view, the first is the standardization of the synthesis methods of 2D TMDs nanosheets. Different parameters and synthesis methods will lead to diverse characteristics, such as size and layer number, which will impact their physicochemical properties and even biological effects. Thus, we need to standardize the preparation of 2D TMDs in a controllable and repeatable manner to obtain the materials with desired structure and property. Moreover, detailed biosafety and toxicity evaluations of these 2D TMDs are urgently demanded from the biosafety point. Although the current evaluation has demonstrated that 2D TMDs exhibit relatively low toxicity, their potential long-term biosafety and in vivo biodegradation in the diverse animal model, and related toxicity mechanisms are still insufficient and should be systemically assessed to reduce the awareness of nanotoxicity.

In conclusion, although the various remarkable progresses of 2D TMDs in biomedical field that has achieved in the last decade are exciting, more research efforts are needed to be undertaken to accelerate the clinical translations of the emerging 2D TMDs.

Acknowledgements The authors gratefully acknowledge the help from Jiani Xie and Shuang Zhu. This work was supported by the National Basic Research Programs of China (Grant Nos. 2016YFA0201600 and 2015CB932104), the National Natural Science Foundation of China (Grant Nos. 31571015, 11621505, 11435002, and 21320102003), and the Youth Innovation Promotion Association CAS (Grant No. 2013007).

Conflict of Interest
The authors declare no conflict of interest.

References

1. Manzeli S, Ovchinnikov D, Pasquier D, Yazyev OV, Kis A (2017) 2D transition metal dichalcogenides. Nat Rev Mater 2:17033. https://doi.org/10.1038/natrevmats.2017.33
2. Tan C, Cao X, Wu XJ, He Q, Yang J, Zhang X, Chen J, Zhao W, Han S, Nam GH, Sindoro M, Zhang H (2017) Recent advances in ultrathin two-dimensional nanomaterials. Chem Rev 117(9):6225–6331. https://doi.org/10.1021/acs.chemrev.6b00558
3. Samadi M, Sarikhani N, Zirak M, Zhang H, Zhang H-L, Moshfegh AZ (2018) Group 6 transition metal dichalcogenide nanomaterials: synthesis, applications and future perspectives. Nanoscale Horiz 3(2):90–204. https://doi.org/10.1039/c7nh00137a
4. Bhimanapati GR, Lin Z, Meunier V, Jung Y, Cha J, Das S, Xiao D, Son Y, Strano MS, Cooper VR, Liang L, Louie SG, Ringe E, Zhou W, Kim SS, Naik RR, Sumpter BG, Terrones H, Xia F, Wang Y, Zhu J, Akinwande D, Alem N, Schuller JA, Schaak RE, Terrones M, Robinson JA (2015) Recent advances in two-dimensional materials beyond graphene. ACS Nano 9(12):11509–11539. https://doi.org/10.1021/acsnano.5b05556
5. Chhowalla M, Shin HS, Eda G, Li LJ, Loh KP, Zhang H (2013) The chemistry of two-dimensional layered transition metal dichalcogenide nanosheets. Nat Chem 5(4):263–275. https://doi.org/10.1038/nchem.1589
6. Kolobov AV, Tominaga J (2016) Emerging applications of 2D TMDCs. In: Two-dimensional transition-metal dichalcogenides. Springer series in materials science, vol 239. Springer International Publishing, Cham, pp 473–512. https://doi.org/10.1007/978-3-319-31450-1_14
7. Chen Y, Tan C, Zhang H, Wang L (2015) Two-dimensional graphene analogues for biomedical applications. Chem Soc Rev 44(9):2681–2701. https://doi.org/10.1039/c4cs00300d
8. Chimene D, Alge DL, Gaharwar AK (2015) Two-dimensional nanomaterials for biomedical applications: emerging trends and future prospects. Adv Mater 27(45):7261–7284. https://doi.org/10.1002/adma.201502422
9. Kurapati R, Kostarelos K, Prato M, Bianco A (2016) Biomedical uses for 2D materials beyond graphene: current advances and challenges ahead. Adv Mater 28(29):6052–6074. https://doi.org/10.1002/adma.201506306
10. Kalantar-zadeh K, Ou JZ, Daeneke T, Strano MS, Pumera M, Gras SL (2015) Two-dimensional transition metal dichalcogenides in biosystems. Adv Funct Mater 25(32):5086–5099. https://doi.org/10.1002/adfm.201500891
11. Liu T, Liu Z (2018) 2D MoS_2 nanostructures for biomedical applications. Adv Healthc Mater 7(8):1701158. https://doi.org/10.1002/adhm.201701158
12. Yang B, Chen Y, Shi J (2018) Material chemistry of two-dimensional inorganic nanosheets in cancer theranostics. Chem 4(6):1284–1313. https://doi.org/10.1016/j.chempr.2018.02.012

13. Li X, Shan J, Zhang W, Su S, Yuwen L, Wang L (2017) Recent advances in synthesis and biomedical applications of two-dimensional transition metal dichalcogenide nanosheets. Small 13(5):1602660. https://doi.org/10.1002/smll.201602660
14. Coleman JN, Lotya M, O'Neill A, Bergin SD, King PJ, Khan U, Young K, Gaucher A, De S, Smith RJ, Shvets IV, Arora SK, Stanton G, Kim HY, Lee K, Kim GT, Duesberg GS, Hallam T, Boland JJ, Wang JJ, Donegan JF, Grunlan JC, Moriarty G, Shmeliov A, Nicholls RJ, Perkins JM, Grieveson EM, Theuwissen K, McComb DW, Nellist PD, Nicolosi V (2011) Two-dimensional nanosheets produced by liquid exfoliation of layered materials. Science 331(6017):568–571. https://doi.org/10.1126/science.1194975
15. Nicolosi V, Chhowalla M, Kanatzidis MG, Strano MS, Coleman JN (2013) Liquid exfoliation of layered materials. Science 340(6139). https://doi.org/10.1126/science.1226419
16. Brent JR, Savjani N, O'Brien P (2017) Synthetic approaches to two-dimensional transition metal dichalcogenide nanosheets. Prog Mater Sci 89:411–478. https://doi.org/10.1016/j.pmatsci.2017.06.002
17. Zhu S, Gong L, Xie J, Gu Z, Zhao Y (2017) Design, synthesis, and surface modification of materials based on transition-metal dichalcogenides for biomedical applications. Small Methods 1(12):1700220. https://doi.org/10.1002/smtd.201700220
18. Yin F, Gu B, Lin Y, Panwar N, Tjin SC, Qu J, Lau SP, Yong K-T (2017) Functionalized 2D nanomaterials for gene delivery applications. Coord Chem Rev 347:77–97. https://doi.org/10.1016/j.ccr.2017.06.024
19. Li Z, Wong SL (2017) Functionalization of 2D transition metal dichalcogenides for biomedical applications. Mater Sci Eng, C 70:1095–1106. https://doi.org/10.1016/j.msec.2016.03.039
20. Cao F, Ju E, Zhang Y, Wang Z, Liu C, Li W, Huang Y, Dong K, Ren J, Qu X (2017) An efficient and benign antimicrobial depot based on silver-infused MoS_2. ACS Nano 11(5):4651–4659. https://doi.org/10.1021/acsnano.7b00343
21. Yin W, Yu J, Lv F, Yan L, Zheng LR, Gu Z, Zhao Y (2016) Functionalized nano-MoS_2 with peroxidase catalytic and near-infrared photothermal activities for safe and synergetic wound antibacterial applications. ACS Nano 10(12):11000–11011. https://doi.org/10.1021/acsnano.6b05810
22. Wang S, Qiu J, Guo W, Yu X, Nie J, Zhang J, Zhang X, Liu Z, Mou X, Li L, Liu H (2017) A nanostructured molybdenum disulfide film for promoting neural stem cell neuronal differentiation: toward a nerve tissue-engineered 3D scaffold. Adv Biosyst 1(5):1600042. https://doi.org/10.1002/adbi.201600042
23. Wang X, Li T, Ma H, Zhai D, Jiang C, Chang J, Wang J, Wu C (2017) A 3D-printed scaffold with MoS_2 nanosheets for tumor therapy and tissue regeneration. NPG Asia Mater 9(4):e376. https://doi.org/10.1038/am.2017.47
24. Choi C, Choi MK, Liu S, Kim MS, Park OK, Im C, Kim J, Qin X, Lee GJ, Cho KW, Kim M, Joh E, Lee J, Son D, Kwon SH, Jeon NL, Song YM, Lu N, Kim DH (2017) Human eye-inspired soft optoelectronic device using high-density MoS_2-graphene curved image sensor array. Nat Commun 8(1):1664. https://doi.org/10.1038/s41467-017-01824-6
25. Gong L, Yan L, Zhou R, Xie J, Wu W, Gu Z (2017) Two-dimensional transition metal dichalcogenide nanomaterials for combination cancer therapy. J Mater Chem B 5(10):1873–1895. https://doi.org/10.1039/c7tb00195a
26. Chen Y, Wang LZ, Shi JL (2016) Two-dimensional non-carbonaceous materials-enabled efficient photothermal cancer therapy. Nano Today 11(3):292–308. https://doi.org/10.1016/j.nantod.2016.05.009
27. Chen H, Liu T, Su Z, Shang L, Wei G (2018) 2D transition metal dichalcogenide nanosheets for photo/thermo-based tumor imaging and therapy. Nanoscale Horiz 3(2):74–89. https://doi.org/10.1039/c7nh00158d
28. Lusic H, Grinstaff MW (2013) X-ray-computed tomography contrast agents. Chem Rev 113(3):1641–1666. https://doi.org/10.1021/cr200358s
29. Gong LJ, Xie JN, Zhu S, Gu ZJ, Zhao YL (2018) Application of multifunctional nanomaterials in tumor radiosensitization. Acta Phys Chim Sin 34(2):140–167. https://doi.org/10.3866/pku.Whxb201707174

30. Wang L, Xiong Q, Xiao F, Duan H (2017) 2D nanomaterials based electrochemical biosensors for cancer diagnosis. Biosens Bioelectron 89(Pt 1):136–151. https://doi.org/10.1016/j.bios.2016.06.011
31. Peng B, Zhang X, Aarts D, Dullens RPA (2018) Superparamagnetic nickel colloidal nanocrystal clusters with antibacterial activity and bacteria binding ability. Nat Nanotechnol 13(6):478–482. https://doi.org/10.1038/s41565-018-0108-0
32. Zheng H, Ma R, Gao M, Tian X, Li Y-Q, Zeng L, Li R (2018) Antibacterial applications of graphene oxides: structure-activity relationships, molecular initiating events and biosafety. Sci Bull 63(2):133–142. https://doi.org/10.1016/j.scib.2017.12.012
33. Le Ouay B, Stellacci F (2015) Antibacterial activity of silver nanoparticles: a surface science insight. Nano Today 10(3):339–354. https://doi.org/10.1016/j.nantod.2015.04.002
34. Chernousova S, Epple M (2013) Silver as antibacterial agent: ion, nanoparticle, and metal. Angew Chem Int Ed 52(6):1636–1653. https://doi.org/10.1002/anie.201205923
35. Franci G, Falanga A, Galdiero S, Palomba L, Rai M, Morelli G, Galdiero M (2015) Silver nanoparticles as potential antibacterial agents. Molecules 20(5):8856–8874. https://doi.org/10.3390/molecules20058856
36. Yang X, Li J, Liang T, Ma C, Zhang Y, Chen H, Hanagata N, Su H, Xu M (2014) Antibacterial activity of two-dimensional MoS2 sheets. Nanoscale 6(17):10126–10133. https://doi.org/10.1039/c4nr01965b
37. Pandit S, Karunakaran S, Boda SK, Basu B, De M (2016) High antibacterial activity of functionalized chemically exfoliated MoS_2. ACS Appl Mater Interfaces 8(46):31567–31573. https://doi.org/10.1021/acsami.6b10916
38. Zhang W, Shi S, Wang Y, Yu S, Zhu W, Zhang X, Zhang D, Yang B, Wang X, Wang J (2016) Versatile molybdenum disulfide based antibacterial composites for in vitro enhanced sterilization and in vivo focal infection therapy. Nanoscale 8(22):11642–11648. https://doi.org/10.1039/c6nr01243d
39. Shang E, Niu J, Li Y, Zhou Y, Crittenden JC (2017) Comparative toxicity of Cd, Mo, and W sulphide nanomaterials toward *E. coli* under UV irradiation. Environ Pollut 224:606–614. https://doi.org/10.1016/j.envpol.2017.02.044
40. Bang GS, Cho S, Son N, Shim GW, Cho BK, Choi SY (2016) DNA-assisted exfoliation of tungsten dichalcogenides and their antibacterial effect. ACS Appl Mater Interfaces 8(3):1943–1950. https://doi.org/10.1021/acsami.5b10136
41. Navale GR, Rout CS, Gohil KN, Dharne MS, Late DJ, Shinde SS (2015) Oxidative and membrane stress-mediated antibacterial activity of WS_2 and rGO-WS_2 nanosheets. RSC Adv 5(91):74726–74733. https://doi.org/10.1039/c5ra15652a
42. Liu X, Duan G, Li W, Zhou Z, Zhou R (2017) Membrane destruction-mediated antibacterial activity of tungsten disulfide (WS_2). RSC Adv 7(60):37873–37880. https://doi.org/10.1039/c7ra06442j
43. Awasthi GP, Adhikari SP, Ko S, Kim HJ, Park CH, Kim CS (2016) Facile synthesis of ZnO flowers modified graphene like MoS_2 sheets for enhanced visible-light-driven photocatalytic activity and antibacterial properties. J Alloys Compd 682:208–215. https://doi.org/10.1016/j.jallcom.2016.04.267
44. Chen CS, Yu WW, Liu TG, Cao SY, Tsang YH (2017) Graphene oxide/WS_2/Mg-doped ZnO nanocomposites for solar-light catalytic and anti-bacterial applications. Sol Energy Mater Sol Cells 160:43–53. https://doi.org/10.1016/j.solmat.2016.10.020
45. Pal A, Jana TK, Roy T, Pradhan A, Maiti R, Choudhury SM, Chatterjee K (2018) MoS_2-TiO_2 nanocomposite with excellent adsorption performance and high antibacterial activity. Chemistryselect 3(1):81–90. https://doi.org/10.1002/slct.201702618
46. Huang X-W, Wei J-J, Liu T, Zhang X-L, Bai S-M, Yang H-H (2017) Silk fibroin-assisted exfoliation and functionalization of transition metal dichalcogenide nanosheets for antibacterial wound dressings. Nanoscale 9(44):17193–17198. https://doi.org/10.1039/c7nr06807g
47. Feng Z, Liu X, Tan L, Cui Z, Yang X, Li Z, Zheng Y, Yeung KWK, Wu S (2018) Electrophoretic deposited stable chitosan@MoS_2 coating with rapid in situ bacteria-killing ability under dual-light irradiation. Small 14(21):1704347. https://doi.org/10.1002/smll.201704347

48. Dubertret B, Skourides P, Norris DJ, Noireaux V, Brivanlou AH, Libchaber A (2002) In vivo imaging of quantum dots encapsulated in phospholipid micelles. Science 298(5599):1759–1762. https://doi.org/10.1126/science.1077194
49. Gao X, Cui Y, Levenson RM, Chung LW, Nie S (2004) In vivo cancer targeting and imaging with semiconductor quantum dots. Nat Biotechnol 22(8):969–976. https://doi.org/10.1038/nbt994
50. Michalet X, Pinaud FF, Bentolila LA, Tsay JM, Doose S, Li JJ, Sundaresan G, Wu AM, Gambhir SS, Weiss S (2005) Quantum dots for live cells, in vivo imaging, and diagnostics. Science 307(5709):538–544. https://doi.org/10.1126/science.1104274
51. Bruns OT, Bischof TS, Harris DK, Franke D, Shi Y, Riedemann L, Bartelt A, Jaworski FB, Carr JA, Rowlands CJ, Wilson MWB, Chen O, Wei H, Hwang GW, Montana DM, Coropceanu I, Achorn OB, Kloepper J, Heeren J, So PTC, Fukumura D, Jensen KF, Jain RK, Bawendi MG (2017) Next-generation in vivo optical imaging with short-wave infrared quantum dots. Nat Biomed Eng 1:0056. https://doi.org/10.1038/s41551-017-0056
52. Oh E, Liu R, Nel A, Gemill KB, Bilal M, Cohen Y, Medintz IL (2016) Meta-analysis of cellular toxicity for cadmium-containing quantum dots. Nat Nanotechnol 11(5):479–486. https://doi.org/10.1038/nnano.2015.338
53. Yang G, Gong H, Liu T, Sun X, Cheng L, Liu Z (2015) Two-dimensional magnetic WS_2@$Fe3O_4$ nanocomposite with mesoporous silica coating for drug delivery and imaging-guided therapy of cancer. Biomaterials 60:62–71. https://doi.org/10.1016/j.biomaterials.2015.04.053
54. Song C, Yang C, Wang F, Ding D, Gao Y, Guo W, Yan M, Liu S, Guo C (2017) MoS_2-Based multipurpose theranostic nanoplatform: realizing dual-imaging-guided combination phototherapy to eliminate solid tumor via a liquefaction necrosis process. J Mater Chem B 5(45):9015–9024. https://doi.org/10.1039/c7tb02648j
55. Dai W, Dong H, Fugetsu B, Cao Y, Lu H, Ma X, Zhang X (2015) Tunable fabrication of molybdenum disulfide quantum dots for intracellular microRNA detection and multiphoton bioimaging. Small 11(33):4158–4164. https://doi.org/10.1002/smll.201500208
56. Gu W, Yan Y, Cao X, Zhang C, Ding C, Xian Y (2016) A facile and one-step ethanol-thermal synthesis of MoS_2 quantum dots for two-photon fluorescence imaging. J Mater Chem B 4(1):27–31. https://doi.org/10.1039/c5tb01839k
57. Chen SC, Lin CY, Cheng TL, Tseng WL (2017) 6-mercaptopurine-induced fluorescence quenching of monolayer MoS_2 nanodots: applications to glutathione sensing, cellular imaging, and glutathione-stimulated drug delivery. Adv Funct Mater 27(41):1702452. https://doi.org/10.1002/adfm.201702452
58. Wang LV, Hu S (2012) Photoacoustic tomography: in vivo imaging from organelles to organs. Science 335(6075):1458–1462. https://doi.org/10.1126/science.1216210
59. Cheng L, Liu J, Gu X, Gong H, Shi X, Liu T, Wang C, Wang X, Liu G, Xing H, Bu W, Sun B, Liu Z (2014) PEGylated WS_2 nanosheets as a multifunctional theranostic agent for in vivo dual-modal CT/photoacoustic imaging guided photothermal therapy. Adv Mater 26(12):1886–1893. https://doi.org/10.1002/adma.201304497
60. Chen JQ, Liu CB, Hu DH, Wang F, Wu HW, Gong XJ, Liu X, Song L, Sheng ZH, Zheng HR (2016) Single-layer MoS_2 nanosheets with amplified photoacoustic effect for highly sensitive photoacoustic imaging of orthotopic brain tumors. Adv Funct Mater 26(47):8715–8725. https://doi.org/10.1002/adfm.201603758
61. Liu T, Wang C, Cui W, Gong H, Liang C, Shi X, Li Z, Sun B, Liu Z (2014) Combined photothermal and photodynamic therapy delivered by PEGylated MoS_2 nanosheets. Nanoscale 6(19):11219–11225. https://doi.org/10.1039/c4nr03753g
62. Liu T, Shi S, Liang C, Shen S, Cheng L, Wang C, Song X, Goel S, Barnhart TE, Cai W, Liu Z (2015) Iron oxide decorated MoS_2 nanosheets with double PEGylation for chelator-free radiolabeling and multimodal imaging guided photothermal therapy. ACS Nano 9(1):950–960. https://doi.org/10.1021/nn506757x
63. Chen L, Zhou X, Nie W, Feng W, Zhang Q, Wang W, Zhang Y, Chen Z, Huang P, He C (2017) Marriage of albumin-gadolinium complexes and MoS_2 nanoflakes as cancer theranostics for

dual-modality magnetic resonance/photoacoustic imaging and photothermal therapy. ACS Appl Mater Interfaces 9(21):17786–17798. https://doi.org/10.1021/acsami.7b04488
64. Liu CB, Chen JQ, Zhu Y, Gong XJ, Zheng RQ, Chen NB, Chen D, Yan HX, Zhang P, Zheng HR, Sheng ZH, Song L (2018) Highly sensitive MoS_2-indocyanine green hybrid for photoacoustic imaging of orthotopic brain glioma at deep site. Nano-Micro Lett 10(3):48. https://doi.org/10.1007/s40820-018-0202-8
65. Wu C, Zhao J, Hu F, Zheng Y, Yang H, Pan S, Shi S, Chen X, Wang S (2018) Design of injectable agar-based composite hydrogel for multi-mode tumor therapy. Carbohydr Polym 180:112–121. https://doi.org/10.1016/j.carbpol.2017.10.024
66. Zhao J, Li J, Zhu C, Hu F, Wu H, Man X, Li Z, Ye C, Zou D, Wang S (2018) Design of phase-changeable and injectable alginate hydrogel for imaging-guided tumor hyperthermia and chemotherapy. ACS Appl Mater Interfaces 10(4):3392–3404. https://doi.org/10.1021/acsami.7b17608
67. Liu T, Chao Y, Gao M, Liang C, Chen Q, Song GS, Cheng L, Liu Z (2016) Ultra-small MoS_2 nanodots with rapid body clearance for photothermal cancer therapy. Nano Res 9(10):3003–3017. https://doi.org/10.1007/s12274-016-1183-x
68. Wang J, Tan X, Pang X, Liu L, Tan F, Li N (2016) MoS_2 quantum dot@polyaniline inorganic-organic nanohybrids for in vivo dual-modal imaging guided synergistic photothermal/radiation therapy. ACS Appl Mater Interfaces 8(37):24331–24338. https://doi.org/10.1021/acsami.6b08391
69. Zhao J, Zhou C, Li M, Li J, Li G, Ma D, Li Z, Zou D (2017) Bottom-up synthesis of ultra-small molybdenum disulfide-polyvinylpyrrolidone nanosheets for imaging-guided tumor regression. Oncotarget 8(63):106707–106720. https://doi.org/10.18632/oncotarget.22477
70. Chen J, Li X, Liu X, Yan H, Xie Z, Sheng Z, Gong X, Wang L, Liu X, Zhang P, Zheng H, Song L, Liu C (2018) Hybrid $MoSe_2$-indocyanine green nanosheets as a highly efficient phototheranostic agent for photoacoustic imaging guided photothermal cancer therapy. Biomater Sci 6(6):1503–1516. https://doi.org/10.1039/c8bm00104a
71. Pan J, Zhu X, Chen X, Zhao Y, Liu J (2018) Gd^{3+}-doped $MoSe_2$ nanosheets used as a theranostic agent for bimodal imaging and highly efficient photothermal cancer therapy. Biomater Sci 6(2):372–387. https://doi.org/10.1039/c7bm00894e
72. Cheng L, Yuan C, Shen S, Yi X, Gong H, Yang K, Liu Z (2015) Bottom-up synthesis of metal-ion-doped WS_2 nanoflakes for cancer theranostics. ACS Nano 9(11):11090–11101. https://doi.org/10.1021/acsnano.5b04606
73. Wang S, Zhao J, Yang H, Wu C, Hu F, Chang H, Li G, Ma D, Zou D, Huang M (2017) Bottom-up synthesis of WS_2 nanosheets with synchronous surface modification for imaging guided tumor regression. Acta Biomater 58:442–454. https://doi.org/10.1016/j.actbio.2017.06.014
74. Zhang C, Yong Y, Song L, Dong X, Zhang X, Liu X, Gu Z, Zhao Y, Hu Z (2016) Multifunctional WS_2@Poly(ethylene imine) nanoplatforms for imaging guided gene-photothermal synergistic therapy of cancer. Adv Healthc Mater 5(21):2776–2787. https://doi.org/10.1002/adhm.201600633
75. Qian XX, Shen SD, Liu T, Cheng L, Liu Z (2015) Two-dimensional TiS_2 nanosheets for in vivo photoacoustic imaging and photothermal cancer therapy. Nanoscale 7(14):6380–6387. https://doi.org/10.1039/c5nr00893j
76. Chen Y, Cheng L, Dong Z, Chao Y, Lei H, Zhao H, Wang J, Liu Z (2017) Degradable vanadium disulfide nanostructures with unique optical and magnetic functions for cancer theranostics. Angew Chem Int Ed 56(42):12991–12996. https://doi.org/10.1002/anie.201707128
77. Shen SD, Chao Y, Dong ZL, Wang GL, Yi X, Song GS, Yang K, Liu Z, Cheng L (2017) Bottom-up preparation of uniform ultrathin rhenium disulfide nanosheets for image-guided photothermal radiotherapy. Adv Funct Mater 27(28):1700250. https://doi.org/10.1002/adfm.201700250
78. Miao ZH, Lv LX, Li K, Liu PY, Li Z, Yang H, Zhao Q, Chang M, Zhen L, Xu CY (2018) Liquid exfoliation of colloidal rhenium disulfide nanosheets as a multifunctional theranostic agent for in vivo photoacoustic/ct imaging and photothermal therapy. Small 14(14):1703789. https://doi.org/10.1002/smll.201703789

79. Wang S, Li X, Chen Y, Cai X, Yao H, Gao W, Zheng Y, An X, Shi J, Chen H (2015) A facile one-pot synthesis of a two-dimensional MoS_2/Bi_2S_3 composite theranostic nanosystem for multi-modality tumor imaging and therapy. Adv Mater 27(17):2775–2782. https://doi.org/10.1002/adma.201500870
80. Yu J, Yin W, Zheng X, Tian G, Zhang X, Bao T, Dong X, Wang Z, Gu Z, Ma X, Zhao Y (2015) Smart MoS_2/Fe_3O_4 nanotheranostic for magnetically targeted photothermal therapy guided by magnetic resonance/photoacoustic imaging. Theranostics 5(9):931–945. https://doi.org/10.7150/thno.11802
81. Liu B, Li C, Chen G, Liu B, Deng X, Wei Y, Xia J, Xing B, Ma P, Lin J (2017) Synthesis and optimization of MoS_2@Fe_3O_4-ICG/Pt(IV) Nanoflowers for MR/IR/PA bioimaging and combined PTT/PDT/chemotherapy triggered by 808 nm laser. Adv Sci 4(8):1600540. https://doi.org/10.1002/advs.201600540
82. Meng XD, Liu ZQ, Cao Y, Dai WH, Zhang K, Dong HF, Feng XY, Zhang XJ (2017) Fabricating aptamer-conjugated PEGylated-MoS_2/Cu1.8S theranostic nanoplatform for multiplexed imaging diagnosis and chemo-photothermal therapy of cancer. Adv Funct Mater 27(16):1605592. https://doi.org/10.1002/adfm.201605592
83. Ke K, Yang W, Xie X, Liu R, Wang LL, Lin WW, Huang G, Lu CH, Yang HH (2017) Copper manganese sulfide nanoplates: a new two-dimensional theranostic nanoplatform for MRI/MSOT dual-modal imaging-guided photothermal therapy in the second near-infrared window. Theranostics 7(19):4763–4776. https://doi.org/10.7150/thno.21694
84. Zhu H, Lai Z, Fang Y, Zhen X, Tan C, Qi X, Ding D, Chen P, Zhang H, Pu K (2017) Ternary chalcogenide nanosheets with ultrahigh photothermal conversion efficiency for photoacoustic theranostics. Small 13(16):1604139. https://doi.org/10.1002/smll.201604139
85. Cui X-Z, Zhou Z-G, Yang Y, Wei J, Wang J, Wang M-W, Yang H, Zhang Y-J, Yang S-P (2015) PEGylated WS_2 nanosheets for X-ray computed tomography imaging and photothermal therapy. Chin Chem Lett 26(6):749–754. https://doi.org/10.1016/j.cclet.2015.03.034
86. Yong Y, Cheng X, Bao T, Zu M, Yan L, Yin W, Ge C, Wang D, Gu Z, Zhao Y (2015) Tungsten sulfide quantum dots as multifunctional nanotheranostics for in vivo dual-modal image-guided photothermal/radiotherapy synergistic therapy. ACS Nano 9(12):12451–12463. https://doi.org/10.1021/acsnano.5b05825
87. Yong Y, Zhou L, Gu Z, Yan L, Tian G, Zheng X, Liu X, Zhang X, Shi J, Cong W, Yin W, Zhao Y (2014) WS_2 nanosheet as a new photosensitizer carrier for combined photodynamic and photothermal therapy of cancer cells. Nanoscale 6(17):10394–10403. https://doi.org/10.1039/C4NR02453B
88. Wang J, Pang X, Tan X, Song Y, Liu L, You Q, Sun Q, Tan F, Li N (2017) A triple-synergistic strategy for combinational photo/radiotherapy and multi-modality imaging based on hyaluronic acid-hybridized polyaniline-coated WS_2 nanodots. Nanoscale 9(17):5551–5564. https://doi.org/10.1039/c6nr09219e
89. Liu Y, Ji X, Liu J, Tong WWL, Askhatova D, Shi J (2017) Tantalum sulfide nanosheets as a theranostic nanoplatform for computed tomography imaging-guided combinatorial chemo-photothermal therapy. Adv Funct Mater 27(39):1703261. https://doi.org/10.1002/adfm.201703261
90. Liu L, Wang J, Tan X, Pang X, You Q, Sun Q, Tan F, Li N (2017) Photosensitizer loaded PEG-MoS_2-Au hybrids for CT/NIRF imaging-guided stepwise photothermal and photodynamic therapy. J Mater Chem B 5(12):2286–2296. https://doi.org/10.1039/c6tb03352k
91. Xu J, Gulzar A, Liu Y, Bi H, Gai S, Liu B, Yang D, He F, Yang P (2017) Integration of IR-808 sensitized upconversion nanostructure and MoS_2 nanosheet for 808 nm NIR light triggered phototherapy and bioimaging. Small 13(36):1701841. https://doi.org/10.1002/smll.201701841
92. Yin W, Yan L, Yu J, Tian G, Zhou L, Zheng X, Zhang X, Yong Y, Li J, Gu Z, Zhao Y (2014) High-throughput synthesis of single-layer MoS_2 nanosheets as a near-infrared photothermal-triggered drug delivery for effective cancer therapy. ACS Nano 8(7):6922–6933. https://doi.org/10.1021/nn501647j

93. Mao B, Bao T, Yu J, Zheng L, Qin J, Yin W, Cao M (2017) One-pot synthesis of MoSe2 hetero-dimensional hybrid self-assembled by nanodots and nanosheets for electrocatalytic hydrogen evolution and photothermal therapy. Nano Res 10(8):2667–2682. https://doi.org/10.1007/s12274-017-1469-7
94. Jing X, Zhi Z, Wang D, Liu J, Shao Y, Meng L (2018) Multifunctional nanoflowers for simultaneous multimodal imaging and high-sensitivity chemo-photothermal treatment. Bioconjug Chem 29(2):559–570. https://doi.org/10.1021/acs.bioconjchem.8b00053
95. Tang S, Fu C, Tan L, Liu T, Mao J, Ren X, Su H, Long D, Chai Q, Huang Z, Chen X, Wang J, Ren J, Meng X (2017) Imaging-guided synergetic therapy of orthotopic transplantation tumor by superselectively arterial administration of microwave-induced microcapsules. Biomaterials 133:144–153. https://doi.org/10.1016/j.biomaterials.2017.04.027
96. Xie W, Gao Q, Wang D, Guo Z, Gao F, Wang X, Cai Q, S-s Feng, Fan H, Sun X, Zhao L (2018) Doxorubicin-loaded Fe_3O_4@MoS_2-PEG-2DG nanocubes as a theranostic platform for magnetic resonance imaging-guided chemo-photothermal therapy of breast cancer. Nano Res 11(5):2470–2487. https://doi.org/10.1007/s12274-017-1871-1
97. Yang G, Zhang R, Liang C, Zhao H, Yi X, Shen S, Yang K, Cheng L, Liu Z (2018) Manganese dioxide coated WS_2@Fe_3O_4/sSiO_2 nanocomposites for pH-responsive MR imaging and oxygen-elevated synergetic therapy. Small 14(2):1702664. https://doi.org/10.1002/smll.201702664
98. Anbazhagan R, Su YA, Tsai HC, Jeng RJ (2016) MoS_2-Gd chelate magnetic nanomaterials with core-shell structure used as contrast agents in in vivo magnetic resonance imaging. ACS Appl Mater Interfaces 8(3):1827–1835. https://doi.org/10.1021/acsami.5b09722
99. Dong X, Yin W, Zhang X, Zhu S, He X, Yu J, Xie J, Guo Z, Yan L, Liu X, Wang Q, Gu Z, Zhao Y (2018) Intelligent MoS_2 nanotheranostic for targeted and enzyme-/pH-/NIR-responsive drug delivery to overcome cancer chemotherapy resistance guided by PET imaging. ACS Appl Mater Interfaces 10(4):4271–4284. https://doi.org/10.1021/acsami.7b17506
100. Chao Y, Wang G, Liang C, Yi X, Zhong X, Liu J, Gao M, Yang K, Cheng L, Liu Z (2016) Rhenium-188 labeled tungsten disulfide nanoflakes for self-sensitized. Near-infrared enhanced radioisotope therapy. Small 12(29):3967–3975. https://doi.org/10.1002/smll.201601375
101. Cheng L, Kamkaew A, Shen S, Valdovinos HF, Sun H, Hernandez R, Goel S, Liu T, Thompson CR, Barnhart TE, Liu Z, Cai W (2016) Facile preparation of multifunctional WS_2/WO_x nanodots for chelator-free Zr-89-labeling and in vivo PET imaging. Small 12(41):5750–5758. https://doi.org/10.1002/smll.201601696
102. Wang SP, Tan LF, Liang P, Liu TL, Wang JZ, Fu CH, Yu J, Dou JP, Hong L, Meng XW (2016) Layered MoS_2 nanoflowers for microwave thermal therapy. J Mater Chem B 4(12):2133–2141. https://doi.org/10.1039/c6tb00296j
103. Liu T, Wang C, Gu X, Gong H, Cheng L, Shi X, Feng L, Sun B, Liu Z (2014) Drug delivery with PEGylated MoS_2 nano-sheets for combined photothermal and chemotherapy of cancer. Adv Mater 26(21):3433–3440. https://doi.org/10.1002/adma.201305256
104. Han Q, Wang X, Jia X, Cai S, Liang W, Qin Y, Yang R, Wang C (2017) CpG loaded MoS_2 nanosheets as multifunctional agents for photothermal enhanced cancer immunotherapy. Nanoscale 9(18):5927–5934. https://doi.org/10.1039/c7nr01460k
105. Wang C, Bai J, Liu YW, Jia XD, Jiang X (2016) Polydopamine coated selenide molybdenum: a new photothermal nanocarrier for highly effective chemo-photothermal synergistic therapy. ACS Biomater Sci Eng 2(11):2011–2017. https://doi.org/10.1021/acsbiomaterials.6b00416
106. Jia XD, Bai J, Ma ZF, Jiang XU (2017) BSA-exfoliated WSe_2 nanosheets as a photoregulated carrier for synergistic photodynamic/photothermal therapy. J Mater Chem B 5(2):269–278. https://doi.org/10.1039/c6tb02525k
107. Huang QL, Wang SR, Zhou J, Zhong XY, Huang YL (2018) Albumin-assisted exfoliated ultrathin rhenium disulfide nanosheets as a tumor targeting and dual-stimuli-responsive drug delivery system for a combination chemo-photothermal treatment. RSC Adv 8(9):4624–4633. https://doi.org/10.1039/c7ra13454a

108. Wust P, Hildebrandt B, Sreenivasa G, Rau B, Gellermann J, Riess H, Felix R, Schlag PM (2002) Hyperthermia in combined treatment of cancer. Lancet Oncol 3(8):487–497. https://doi.org/10.1016/s1470-2045(02)00818-5
109. Chou SS, Kaehr B, Kim J, Foley BM, De M, Hopkins PE, Huang J, Brinker CJ, Dravid VP (2013) Chemically exfoliated MoS_2 as near-infrared photothermal agents. Angew Chem Int Ed 52(15):4160–4164. https://doi.org/10.1002/anie.201209229
110. Robinson JT, Welsher K, Tabakman SM, Sherlock SP, Wang H, Luong R, Dai H (2010) High performance in vivo near-IR (>1 μm) imaging and photothermal cancer therapy with carbon nanotubes. Nano Res 3(11):779–793. https://doi.org/10.1007/s12274-010-0045-1
111. Wang S, Li K, Chen Y, Chen H, Ma M, Feng J, Zhao Q, Shi J (2015) Biocompatible PEGylated MoS_2 nanosheets: controllable bottom-up synthesis and highly efficient photothermal regression of tumor. Biomaterials 39:206–217. https://doi.org/10.1016/j.biomaterials.2014.11.009
112. Li M, Zhao AD, Dong K, Li W, Ren JS, Qu XG (2015) Chemically exfoliated WS_2 nanosheets efficiently inhibit amyloid beta-peptide aggregation and can be used for photothermal treatment of Alzheimer's disease. Nano Res 8(10):3216–3227. https://doi.org/10.1007/s12274-015-0821-z
113. Han Q, Cai S, Yang L, Wang X, Qi C, Yang R, Wang C (2017) Molybdenum disulfide nanoparticles as multifunctional inhibitors against Alzheimer's disease. ACS Appl Mater Interfaces 9(25):21116–21123. https://doi.org/10.1021/acsami.7b03816
114. Zhang H, Chen H-J, Du X, Wen D (2014) Photothermal conversion characteristics of gold nanoparticle dispersions. Sol Energy 100:141–147. https://doi.org/10.1016/j.solener.2013.12.004
115. Lin H, Gao S, Dai C, Chen Y, Shi J (2017) A two-dimensional biodegradable niobium carbide (MXene) for photothermal tumor eradication in NIR-I and NIR-II biowindows. J Am Chem Soc 139(45):16235–16247. https://doi.org/10.1021/jacs.7b07818
116. Lei Z, Zhu W, Xu S, Ding J, Wan J, Wu P (2016) Hydrophilic $MoSe_2$ nanosheets as effective photothermal therapy agents and their application in smart devices. ACS Appl Mater Interfaces 8(32):20900–20908. https://doi.org/10.1021/acsami.6b07326
117. Lin H, Wang Y, Gao S, Chen Y, Shi J (2018) Theranostic 2D tantalum carbide (MXene). Adv Mater 30(4):1703284. https://doi.org/10.1002/adma.201703284
118. Sun Z, Xie H, Tang S, Yu XF, Guo Z, Shao J, Zhang H, Huang H, Wang H, Chu PK (2015) Ultrasmall black phosphorus quantum dots: synthesis and use as photothermal agents. Angew Chem Int Ed 54(39):11526–11530. https://doi.org/10.1002/anie.201506154
119. Hessel CM, Pattani VP, Rasch M, Panthani MG, Koo B, Tunnell JW, Korgel BA (2011) Copper selenide nanocrystals for photothermal therapy. Nano Lett 11(6):2560–2566. https://doi.org/10.1021/nl201400z
120. Zeng J, Goldfeld D, Xia Y (2013) A plasmon-assisted optofluidic (PAOF) system for measuring the photothermal conversion efficiencies of gold nanostructures and controlling an electrical switch. Angew Chem Int Ed 52(15):4169–4173. https://doi.org/10.1002/anie.201210359
121. Wang B, Wang JH, Liu Q, Huang H, Chen M, Li K, Li C, Yu XF, Chu PK (2014) Rose-bengal-conjugated gold nanorods for in vivo photodynamic and photothermal oral cancer therapies. Biomaterials 35(6):1954–1966. https://doi.org/10.1016/j.biomaterials.2013.11.066
122. Feng W, Chen L, Qin M, Zhou X, Zhang Q, Miao Y, Qiu K, Zhang Y, He C (2015) Flower-like PEGylated MoS_2 nanoflakes for near-infrared photothermal cancer therapy. Sci Rep 5:17422. https://doi.org/10.1038/srep17422
123. Huang Z, Qi Y, Yu D, Zhan J (2016) Radar-like MoS_2 nanoparticles as a highly efficient 808 nm laser-induced photothermal agent for cancer therapy. RSC Adv 6(37):31031–31036. https://doi.org/10.1039/C6RA03226E
124. Li X, Gong Y, Zhou XQ, Jin H, Yan HH, Wang SG, Liu J (2016) Facile synthesis of soybean phospholipid-encapsulated MoS_2 nanosheets for efficient in vitro and in vivo photothermal regression of breast tumor. Int J Nanomed 11:1819–1833. https://doi.org/10.2147/ijn.s104198

125. Tan LF, Wang SP, Xu K, Liu TL, Liang P, Niu M, Fu CH, Shao HB, Yu J, Ma TC, Ren XL, Li H, Dou JP, Ren J, Meng XW (2016) Layered MoS_2 hollow spheres for highly-efficient photothermal therapy of rabbit liver orthotopic transplantation tumors. Small 12(15):2046–2055. https://doi.org/10.1002/smll.201600191
126. Ariyasu S, Mu J, Zhang X, Huang Y, Yeow EKL, Zhang H, Xing B (2017) Investigation of thermally induced cellular ablation and heat response triggered by planar MoS_2-based nanocomposite. Bioconjug Chem 28(4):1059–1067. https://doi.org/10.1021/acs.bioconjchem.6b00741
127. Chen L, Feng Y, Zhou X, Zhang Q, Nie W, Wang W, Zhang Y, He C (2017) One-pot synthesis of MoS_2 nanoflakes with desirable degradability for photothermal cancer therapy. ACS Appl Mater Interfaces 9(20):17347–17358. https://doi.org/10.1021/acsami.7b02657
128. Huang B, Wang D, Wang G, Zhang F, Zhou L (2017) Enhancing the colloidal stability and surface functionality of molybdenum disulfide (MoS_2) nanosheets with hyperbranched polyglycerol for photothermal therapy. J Colloid Interface Sci 508:214–221. https://doi.org/10.1016/j.jcis.2017.08.062
129. Li Z, Yang Y, Yao J, Shao Z, Chen X (2017) A facile fabrication of silk/MoS_2 hybrids for photothermal therapy. Mater Sci Eng C Mater Biol Appl 79:123–129. https://doi.org/10.1016/j.msec.2017.05.010
130. Park CH, Yun H, Yang H, Lee J, Kim BJ (2017) Fluorescent block copolymer-MoS_2 nanocomposites for real-time photothermal heating and imaging. Adv Funct Mater 27(5):1604403. https://doi.org/10.1002/adfm.201604403
131. Zhang Y, Xiu W, Sun Y, Zhu D, Zhang Q, Yuwen L, Weng L, Teng Z, Wang L (2017) RGD-QD-MoS_2 nanosheets for targeted fluorescent imaging and photothermal therapy of cancer. Nanoscale 9(41):15835–15845. https://doi.org/10.1039/c7nr05278b
132. Zhang YB, Jia GZ, Wang P, Zhang Q, Wei XY, Dong EM, Yao JH (2017) Size effect on near infrared photothermal conversion properties of liquid-exfoliated MoS_2 and MoSe2. Superlattices Microstruct 105:22–27. https://doi.org/10.1016/j.spmi.2016.11.058
133. Park CH, Lee S, Pornnoppadol G, Nam YS, Kim SH, Kim BJ (2018) Microcapsules containing pH-responsive, fluorescent polymer-integrated MoS_2: an effective platform for in situ pH sensing and photothermal heating. ACS Appl Mater Interfaces 10(10):9023–9031. https://doi.org/10.1021/acsami.7b19468
134. Liu Q, Sun C, He Q, Khalil A, Xiang T, Liu D, Zhou Y, Wang J, Song L (2015) Stable metallic 1T-WS_2 ultrathin nanosheets as a promising agent for near-infrared photothermal ablation cancer therapy. Nano Res 8(12):3982–3991. https://doi.org/10.1007/s12274-015-0901-0
135. Macharia DK, Yu N, Zhong R, Xiao Z, Yang J, Chen Z (2016) Synthesis of WS_2 nanowires as efficient 808 nm-laser-driven photothermal nanoagents. J Nanosci Nanotechnol 16(6):5865–5868. https://doi.org/10.1166/jnn.2016.11747
136. Nandi S, Bhunia SK, Zeiri L, Pour M, Nachman I, Raichman D, Lellouche JM, Jelinek R (2017) Bifunctional carbon-dot-WS_2 nanorods for photothermal therapy and cell imaging. Chem Eur J 23(4):963–969. https://doi.org/10.1002/chem.201604787
137. Yuwen LH, Zhou JJ, Zhang YQ, Zhang Q, Shan JY, Luo ZM, Weng LX, Teng ZG, Wang LH (2016) Aqueous phase preparation of ultrasmall $MoSe_2$ nanodots for efficient photothermal therapy of cancer cells. Nanoscale 8(5):2720–2726. https://doi.org/10.1039/c5nr08166a
138. Zhong CL, Zhao X, Wang LJ, Li YX, Zhao YY (2017) Facile synthesis of biocompatible $MoSe_2$ nanoparticles for efficient targeted photothermal therapy of human lung cancer. RSC Adv 7(12):7382–7391. https://doi.org/10.1039/c6ra27384j
139. Zhu Z, Zou Y, Hu W, Li Y, Gu Y, Cao B, Guo N, Wang L, Song J, Zhang S, Gu H, Zeng H (2016) Near-infrared plasmonic 2D semimetals for applications in communication and biology. Adv Funct Mater 26(11):1793–1802. https://doi.org/10.1002/adfm.201504884
140. Ren QL, Li B, Peng ZY, He GJ, Zhang WL, Guan GQ, Huang XJ, Xiao ZY, Liao LJ, Pan YS, Yang XJ, Zou RJ, Hu JQ (2016) SnS nanosheets for efficient photothermal therapy. New J Chem 40(5):4464–4467. https://doi.org/10.1039/c5nj03263f
141. Ma N, Zhang M-K, Wang X-S, Zhang L, Feng J, Zhang X-Z (2018) NIR light-triggered degradable $MoTe_2$ nanosheets for combined photothermal and chemotherapy of cancer. Adv Funct Mater:1801139. https://doi.org/10.1002/adfm.201801139

142. Lin H, Wang X, Yu L, Chen Y, Shi J (2017) Two-dimensional ultrathin MXene ceramic nanosheets for photothermal conversion. Nano Lett 17(1):384–391. https://doi.org/10.1021/acs.nanolett.6b04339
143. Xie H, Li Z, Sun Z, Shao J, Yu XF, Guo Z, Wang J, Xiao Q, Wang H, Wang QQ, Zhang H, Chu PK (2016) Metabolizable ultrathin bi2se3 nanosheets in imaging-guided photothermal therapy. Small 12(30):4136–4145. https://doi.org/10.1002/smll.201601050
144. Robinson JT, Tabakman SM, Liang Y, Wang H, Casalongue HS, Vinh D, Dai H (2011) Ultrasmall reduced graphene oxide with high near-infrared absorbance for photothermal therapy. J Am Chem Soc 133(17):6825–6831. https://doi.org/10.1021/ja2010175
145. Xia C, Wang H, Jiao F, Gao F, Wu Q, Shen Y, Zhang Y, Qian X (2018) Rational synthesis of MoS_2-based immobilized trypsin for rapid and effective protein digestion. Talanta 179:393–400. https://doi.org/10.1016/j.talanta.2017.11.027
146. Bettaieb A, Wrzal PK, Averill-Bates DA (2013) Hyperthermia: cancer treatment and beyond. In: Cancer treatment—conventional and innovative approaches. https://doi.org/10.5772/55795
147. Day ES, Morton JG, West JL (2009) Nanoparticles for thermal cancer therapy. J Biomech Eng 131(7):074001–074005. https://doi.org/10.1115/1.3156800
148. Weissleder R (2001) A clearer vision for in vivo imaging. Nat Biotechnol 19(4):316–317. https://doi.org/10.1038/86684
149. Yun SH, Kwok SJJ (2017) Light in diagnosis, therapy and surgery. Nat Biomed Eng 1(1):0008. https://doi.org/10.1038/s41551-016-0008
150. Qian GJ, Wang N, Shen Q, Sheng YH, Zhao JQ, Kuang M, Liu GJ, Wu MC (2012) Efficacy of microwave versus radiofrequency ablation for treatment of small hepatocellular carcinoma: experimental and clinical studies. Eur Radiol 22(9):1983–1990. https://doi.org/10.1007/s00330-012-2442-1
151. Fu C, He F, Tan L, Ren X, Zhang W, Liu T, Wang J, Ren J, Chen X, Meng X (2017) MoS_2 nanosheets encapsulated in sodium alginate microcapsules as microwave embolization agents for large orthotopic transplantation tumor therapy. Nanoscale 9(39):14846–14853. https://doi.org/10.1039/c7nr04274d
152. Agostinis P, Berg K, Cengel KA, Foster TH, Girotti AW, Gollnick SO, Hahn SM, Hamblin MR, Juzeniene A, Kessel D, Korbelik M, Moan J, Mroz P, Nowis D, Piette J, Wilson BC, Golab J (2011) Photodynamic therapy of cancer: an update. CA Cancer J Clin 61(4):250–281. https://doi.org/10.3322/caac.20114
153. Ji DK, Zhang Y, Zang Y, Li J, Chen GR, He XP, Tian H (2016) Targeted intracellular production of reactive oxygen species by a 2D molybdenum disulfide glycosheet. Adv Mater 28(42):9356–9363. https://doi.org/10.1002/adma.201602748
154. Dong H, Tang S, Hao Y, Yu H, Dai W, Zhao G, Cao Y, Lu H, Zhang X, Ju H (2016) Fluorescent MoS_2 quantum dots: ultrasonic preparation, up-conversion and down-conversion bioimaging, and photodynamic therapy. ACS Appl Mater Interfaces 8(5):3107–3114. https://doi.org/10.1021/acsami.5b10459
155. Peng MY, Zheng DW, Wang SB, Cheng SX, Zhang XZ (2017) Multifunctional nanosystem for synergistic tumor therapy delivered by two-dimensional MoS_2. ACS Appl Mater Interfaces 9(16):13965–13975. https://doi.org/10.1021/acsami.7b03276
156. Jia L, Ding L, Tian J, Bao L, Hu Y, Ju H, Yu JS (2015) Aptamer loaded MoS_2 nanoplates as nanoprobes for detection of intracellular ATP and controllable photodynamic therapy. Nanoscale 7(38):15953–15961. https://doi.org/10.1039/c5nr02224j
157. Han J, Xia H, Wu Y, Kong SN, Deivasigamani A, Xu R, Hui KM, Kang Y (2016) Single-layer MoS_2 nanosheet grafted upconversion nanoparticles for near-infrared fluorescence imaging-guided deep tissue cancer phototherapy. Nanoscale 8(15):7861–7865. https://doi.org/10.1039/c6nr00150e
158. Chen L, Feng W, Zhou X, Qiu K, Miao Y, Zhang Q, Qin M, Li L, Zhang Y, He C (2016) Facile synthesis of novel albumin-functionalized flower-like MoS_2 nanoparticles for in vitro chemo-photothermal synergistic therapy. RSC Adv 6(16):13040–13049. https://doi.org/10.1039/C5RA27822H

159. Deng R, Yi H, Fan FY, Fu L, Zeng Y, Wang Y, Li YC, Liu YL, Ji SJ, Su Y (2016) Facile exfoliation of MoS_2 nanosheets by protein as a photothermal-triggered drug delivery system for synergistic tumor therapy. RSC Adv 6(80):77083–77092. https://doi.org/10.1039/c6ra13993k
160. Shao T, Wen J, Zhang Q, Zhou Y, Liu L, Yuwen L, Tian Y, Zhang Y, Tian W, Su Y, Teng Z, Lu G, Xu J (2016) NIR photoresponsive drug delivery and synergistic chemo-photothermal therapy by monodispersed-MoS_2-nanosheets wrapped periodic mesoporous organosilicas. J Mater Chem B 4(47):7708–7717. https://doi.org/10.1039/c6tb02724e
161. Lei Q, Wang SB, Hu JJ, Lin YX, Zhu CH, Rong L, Zhang XZ (2017) Stimuli-Responsive "Cluster Bomb" for Programmed Tumor Therapy. ACS Nano 11(7):7201–7214. https://doi.org/10.1021/acsnano.7b03088
162. Wang KW, Chen QQ, Xue W, Li S, Liu ZH (2017) Combined chemo-photothermal antitumor therapy using molybdenum disulfide modified with hyperbranched polyglycidyl. ACS Biomater Sci Eng 3(10):2325–2335. https://doi.org/10.1021/acsbiomaterials.7b00499
163. Liao W, Zhang L, Zhong Y, Shen Y, Li C, An N (2018) Fabrication of ultrasmall WS_2 quantum dots-coated periodic mesoporous organosilica nanoparticles for intracellular drug delivery and synergistic chemo-photothermal therapy. Onco Targets Ther 11:1949–1960. https://doi.org/10.2147/OTT.S160748
164. Wang S, Chen Y, Li X, Gao W, Zhang L, Liu J, Zheng Y, Chen H, Shi J (2015) Injectable 2D MoS_2-integrated drug delivering implant for highly efficient NIR-triggered synergistic tumor hyperthermia. Adv Mater 27(44):7117–7122. https://doi.org/10.1002/adma.201503869
165. Zhang A, Li A, Tian W, Li Z, Wei C, Sun Y, Zhao W, Liu M, Liu J (2017) A target-directed chemo-photothermal system based on transferrin and copolymer-modified MoS_2 nanoplates with pH-activated drug release. Chem Eur J 23(47):11346–11356. https://doi.org/10.1002/chem.201701916
166. Zhao W, Li AH, Chen C, Quan FY, Sun L, Zhang AT, Zheng YW, Liu JQ (2017) Transferrin-decorated, MoS_2-capped hollow mesoporous silica nanospheres as a self-guided chemo-photothermal nanoplatform for controlled drug release and thermotherapy. J Mater Chem B 5(35):7403–7414. https://doi.org/10.1039/c7tb01648d
167. Zhang A, Li A, Zhao W, Yan G, Liu B, Liu M, Li M, Huo B, Liu J (2018) An efficient and self-guided chemo-photothermal drug loading system based on copolymer and transferrin decorated MoS_2 nanodots for dually controlled drug release. Chem Eng J 342:120–132. https://doi.org/10.1016/j.cej.2018.02.081
168. Mellman I, Coukos G, Dranoff G (2011) Cancer immunotherapy comes of age. Nature 480(7378):480–489. https://doi.org/10.1038/nature10673
169. Song W, Musetti SN, Huang L (2017) Nanomaterials for cancer immunotherapy. Biomaterials 148:16–30. https://doi.org/10.1016/j.biomaterials.2017.09.017
170. Wang ZJ, Liu WH, Shi JY, Chen N, Fan CH (2018) Nanoscale delivery systems for cancer immunotherapy. Mater Horiz 5(3):344–362. https://doi.org/10.1039/c7mh00991g
171. Ge R, Liu C, Zhang X, Wang W, Li B, Liu J, Liu Y, Sun H, Zhang D, Hou Y, Zhang H, Yang B (2018) Photothermal-activatable Fe_3O_4 superparticle nanodrug carriers with PD-L1 immune checkpoint blockade for anti-metastatic cancer immunotherapy. ACS Appl Mater Interfaces 10(24):20342–20355. https://doi.org/10.1021/acsami.8b05876
172. Lu K, He C, Guo N, Chan C, Ni K, Weichselbaum RR, Lin W (2016) Chlorin-based nanoscale metal-organic framework systemically rejects colorectal cancers via synergistic photodynamic therapy and checkpoint blockade immunotherapy. J Am Chem Soc 138(38):12502–12510. https://doi.org/10.1021/jacs.6b06663
173. Ni K, Lan G, Chan C, Quigley B, Lu K, Aung T, Guo N, La Riviere P, Weichselbaum RR, Lin W (2018) Nanoscale metal-organic frameworks enhance radiotherapy to potentiate checkpoint blockade immunotherapy. Nat Commun 9(1):2351. https://doi.org/10.1038/s41467-018-04703-w
174. Lan G, Ni K, Xu Z, Veroneau SS, Song Y, Lin W (2018) Nanoscale metal-organic framework overcomes hypoxia for photodynamic therapy primed cancer immunotherapy. J Am Chem Soc 140(17):5670–5673. https://doi.org/10.1021/jacs.8b01072

175. He C, Duan X, Guo N, Chan C, Poon C, Weichselbaum RR, Lin W (2016) Core-shell nanoscale coordination polymers combine chemotherapy and photodynamic therapy to potentiate checkpoint blockade cancer immunotherapy. Nat Commun 7:12499. https://doi.org/10.1038/ncomms12499
176. Noh YW, Kim SY, Kim JE, Kim S, Ryu J, Kim I, Lee E, Um SH, Lim YT (2017) Multifaceted immunomodulatory nanoliposomes: reshaping tumors into vaccines for enhanced cancer immunotherapy. Adv Funct Mater 27(8):1605398. https://doi.org/10.1002/adfm.201605398
177. Zhu G, Liu Y, Yang X, Kim YH, Zhang H, Jia R, Liao HS, Jin A, Lin J, Aronova M, Leapman R, Nie Z, Niu G, Chen X (2016) DNA-inorganic hybrid nanovaccine for cancer immunotherapy. Nanoscale 8(12):6684–6692. https://doi.org/10.1039/c5nr08821f
178. Pardo M, Shuster-Meiseles T, Levin-Zaidman S, Rudich A, Rudich Y (2014) Low cytotoxicity of inorganic nanotubes and fullerene-like nanostructures in human bronchial epithelial cells: relation to inflammatory gene induction and antioxidant response. Environ Sci Technol 48(6):3457–3466. https://doi.org/10.1021/es500065z
179. Rajendrakumar SK, Uthaman S, Cho CS, Park IK (2018) Nanoparticle-based phototriggered cancer immunotherapy and its domino effect in the tumor microenvironment. Biomacromol 19(6):1869–1887. https://doi.org/10.1021/acs.biomac.8b00460
180. Wang H, Mu X, He H, Zhang XD (2018) Cancer radiosensitizers. Trends Pharmacol Sci 39(1):24–48. https://doi.org/10.1016/j.tips.2017.11.003
181. Zhu S, Gu Z, Zhao Y (2018) Harnessing tumor microenvironment for nanoparticle-mediated radiotherapy. Adv Therap 0(0):1800050. https://doi.org/10.1002/adtp.201800050
182. Xie J, Wang N, Dong X, Wang C, Du Z, Mei L, Yong Y, Huang C, Li Y, Gu Z, Zhao Y (2018) Graphdiyne nanoparticles with high free radical scavenging activity for radiation protection. ACS Appl Mater Interfaces. https://doi.org/10.1021/acsami.8b00949
183. Xie J, Wang C, Zhao F, Gu Z, Zhao Y (2018) Application of multifunctional nanomaterials in radioprotection of healthy tissues. Adv Healthc Mater 0(0):1800421. https://doi.org/10.1002/adhm.201800421
184. Hall EJ, Giaccia AJ (2012) Radiobiology for the radiologist. Wolters Kluwer Health
185. Kouvaris JR, Kouloulias VE, Vlahos LJ (2007) Amifostine: the first selective-target and broad-spectrum radioprotector. Oncologist 12(6):738–747. https://doi.org/10.1634/theoncologist.12-6-738
186. Grdina DJ, Murley JS, Kataoka Y (2002) Radioprotectants: current status and new directions. Oncology 63(Suppl. 2):2–10. https://doi.org/10.1159/000067146
187. Tarnuzzer RW, Colon J, Patil S, Seal S (2005) Vacancy engineered ceria nanostructures for protection from radiation-induced cellular damage. Nano Lett 5(12):2573–2577. https://doi.org/10.1021/nl052024f
188. Colon J, Hsieh N, Ferguson A, Kupelian P, Seal S, Jenkins DW, Baker CH (2010) Cerium oxide nanoparticles protect gastrointestinal epithelium from radiation-induced damage by reduction of reactive oxygen species and upregulation of superoxide dismutase 2. Nanomed Nanotechnol Biol Med 6(5):698–705. https://doi.org/10.1016/j.nano.2010.01.010
189. Xue Y, Luan Q, Yang D, Yao X, Zhou K (2011) Direct evidence for hydroxyl radical scavenging activity of cerium oxide nanoparticles. J Phys Chem C 115(11):4433–4438. https://doi.org/10.1021/jp109819u
190. Li H, Yang ZY, Liu C, Zeng YP, Hao YH, Gu Y, Wang WD, Li R (2015) PEGylated ceria nanoparticles used for radioprotection on human liver cells under gamma-ray irradiation. Free Radic Biol Med 87:26–35. https://doi.org/10.1016/j.freeradbiomed.2015.06.010
191. Xie J, Yong Y, Dong X, Du J, Guo Z, Gong L, Zhu S, Tian G, Yu S, Gu Z, Zhao Y (2017) Therapeutic nanoparticles based on curcumin and bamboo charcoal nanoparticles for chemo-photothermal synergistic treatment of cancer and radioprotection of normal cells. ACS Appl Mater Interfaces 9(16):14281–14291. https://doi.org/10.1021/acsami.7b02622
192. Cirillo G, Hampel S, Klingeler R, Puoci F, Iemma F, Curcio M, Parisi Ortensia I, Spizzirri Umile G, Picci N, Leonhardt A, Ritschel M, Büchner B (2010) Antioxidant multi-walled carbon nanotubes by free radical grafting of gallic acid: new materials for biomedical applications. J Pharm Pharmacol 63(2):179–188. https://doi.org/10.1111/j.2042-7158.2010.01211.x

193. Qiu Y, Wang Z, Owens ACE, Kulaots I, Chen Y, Kane AB, Hurt RH (2014) Antioxidant chemistry of graphene-based materials and its role in oxidation protection technology. Nanoscale 6(20):11744–11755. https://doi.org/10.1039/C4NR03275F
194. Yim D, Kim JE, Kim HI, Yang JK, Kang TW, Nam J, Han SH, Jun B, Lee CH, Lee SU, Kim JW, Kim JH (2018) Adjustable intermolecular interactions allowing 2D transition metal dichalcogenides with prolonged scavenging activity for reactive oxygen species. Small 14(16):1800026. https://doi.org/10.1002/smll.201800026
195. Zhang XD, Zhang J, Wang J, Yang J, Chen J, Shen X, Deng J, Deng D, Long W, Sun YM, Liu C, Li M (2016) Highly catalytic nanodots with renal clearance for radiation protection. ACS Nano 10(4):4511–4519. https://doi.org/10.1021/acsnano.6b00321
196. Bai XT, Wang JY, Mu XY, Yang J, Liu HX, Xu FJ, Jing YQ, Liu LF, Xue XH, Dai HT, Liu Q, Sun YM, Liu CL, Zhang XD (2017) Ultrasmall WS_2 quantum dots with visible fluorescence for protection of cells and animal models from radiation-induced damages. ACS Biomater Sci Eng 3(3):460–470. https://doi.org/10.1021/acsbiomaterials.6b00714
197. Liu HX, Wang JY, Jing YQ, Yang J, Bai XT, Mu XY, Xu FJ, Xue XH, Liu LF, Sun YM, Liu Q, Dai HT, Liu CL, Zhang XD (2017) Renal clearable luminescent WSe_2 for radioprotection of nontargeted tissues during radiotherapy. Part Part Syst Charact 34(6):1700035. https://doi.org/10.1002/ppsc.201700035
198. Radioprotection: taking the Toll Road (2008). Science 320 (5873):151–151. https://doi.org/10.1126/science.320.5873.151g
199. Fan W, Yung B, Huang P, Chen X (2017) Nanotechnology for multimodal synergistic cancer therapy. Chem Rev 117(22):13566–13638. https://doi.org/10.1021/acs.chemrev.7b00258
200. Zhang L, Webster TJ (2009) Nanotechnology and nanomaterials: Promises for improved tissue regeneration. Nano Today 4(1):66–80. https://doi.org/10.1016/j.nantod.2008.10.014
201. Lalwani G, Henslee AM, Farshid B, Parmar P, Lin L, Qin YX, Kasper FK, Mikos AG, Sitharaman B (2013) Tungsten disulfide nanotubes reinforced biodegradable polymers for bone tissue engineering. Acta Biomater 9(9):8365–8373. https://doi.org/10.1016/j.actbio.2013.05.018
202. Jaiswal MK, Carrow JK, Gentry JL, Gupta J, Altangerel N, Scully M, Gaharwar AK (2017) Vacancy-driven gelation using defect-rich nanoassemblies of 2D transition metal dichalcogenides and polymeric binder for biomedical applications. Adv Mater 29(36):1702037. https://doi.org/10.1002/adma.201702037
203. Wu S, Wang J, Jin L, Li Y, Wang Z (2018) Effects of polyacrylonitrile/MoS_2 composite nanofibers on the growth behavior of bone marrow mesenchymal stem cells. ACS Appl Nano Mater 1(1):337–343. https://doi.org/10.1021/acsanm.7b00188
204. Hussey GS, Dziki JL, Badylak SF (2018) Extracellular matrix-based materials for regenerative medicine. Nat Rev Mater 3(7):159–173. https://doi.org/10.1038/s41578-018-0023-x
205. Jiang B, Duan D, Gao L, Zhou M, Fan K, Tang Y, Xi J, Bi Y, Tong Z, Gao GF, Xie N, Tang A, Nie G, Liang M, Yan X (2018) Standardized assays for determining the catalytic activity and kinetics of peroxidase-like nanozymes. Nat Protoc 13(7):1506–1520. https://doi.org/10.1038/s41596-018-0001-1
206. Zhu X, Ji X, Kong N, Chen Y, Mahmoudi M, Xu X, Ding L, Tao W, Cai T, Li Y, Gan T, Barrett A, Bharwani Z, Chen H, Farokhzad OC (2018) Intracellular mechanistic understanding of 2D MoS_2 nanosheets for anti-exocytosis-enhanced synergistic cancer therapy. ACS Nano 12(3):2922–2938. https://doi.org/10.1021/acsnano.8b00516
207. Yan L, Zhao YL, Gu ZJ (2016) Nanotoxicity of near infrared nanomaterials. In: Near-infrared nanomaterials: preparation, bioimaging and therapy applications. The Royal Society of Chemistry, pp 355–402. (Chapter 11). https://doi.org/10.1039/9781782623939-00355
208. Ling Y, Gu Z, S-g Kang, Luo J, Zhou R (2016) Structural damage of a β-sheet protein upon adsorption onto molybdenum disulfide nanotubes. J Phys Chem C 120(12):6796–6803. https://doi.org/10.1021/acs.jpcc.5b11236
209. Gu Z, Yang Z, Kang SG, Yang JR, Luo J, Zhou R (2016) Robust denaturation of villin headpiece by MoS_2 nanosheet: potential molecular origin of the nanotoxicity. Sci Rep 6:28252. https://doi.org/10.1038/srep28252

210. Gu Z, Plant LD, Meng X-Y, Perez-Aguilar JM, Wang Z, Dong M, Logothetis DE, Zhou R (2018) Exploring the nanotoxicology of MoS_2: a study on the interaction of mos2 nanoflakes and K^+ channels. ACS Nano 12(1):705–717. https://doi.org/10.1021/acsnano.7b07871
211. Zou W, Zhang X, Zhao M, Zhou Q, Hu X (2017) Cellular proliferation and differentiation induced by single-layer molybdenum disulfide and mediation mechanisms of proteins via the Akt-mTOR-p70S6K signaling pathway. Nanotoxicology 11(6):781–793. https://doi.org/10.1080/17435390.2017.1357213
212. Kenry Lim CT (2017) Biocompatibility and nanotoxicity of layered two-dimensional nanomaterials. Chemnanomat 3(1):5–16. https://doi.org/10.1002/cnma.201600290
213. Wei Y, Quan L, Zhou C, Zhan Q (2018) Factors relating to the biodistribution & clearance of nanoparticles & their effects on in vivo application. Nanomedicine (Lond) 13(12):1495–1512. https://doi.org/10.2217/nnm-2018-0040
214. Chng EL, Sofer Z, Pumera M (2014) MoS_2 exhibits stronger toxicity with increased exfoliation. Nanoscale 6(23):14412–14418. https://doi.org/10.1039/c4nr04907a
215. Wang X, Mansukhani ND, Guiney LM, Ji Z, Chang CH, Wang M, Liao YP, Song TB, Sun B, Li R, Xia T, Hersam MC, Nel AE (2015) Differences in the toxicological potential of 2D versus aggregated molybdenum disulfide in the lung. Small 11(38):5079–5087. https://doi.org/10.1002/smll.201500906
216. Latiff NM, Sofer Z, Fisher AC, Pumera M (2017) Cytotoxicity of exfoliated layered vanadium dichalcogenides. Chem Eur J 23(3):684–690. https://doi.org/10.1002/chem.201604430
217. Appel JH, Li DO, Podlevsky JD, Debnath A, Green AA, Wang QH, Chae J (2016) Low cytotoxicity and genotoxicity of two-dimensional MoS_2 and WS_2. ACS Biomater Sci Eng 2(3):361–367. https://doi.org/10.1021/acsbiomaterials.5b00467
218. Rosli NF, Latiff NM, Sofer Z, Fisher AC, Pumera M (2018) In vitro cytotoxicity of covalently protected layered molybdenum disulfide. Appl Mater Today 11:200–206. https://doi.org/10.1016/j.apmt.2018.02.001
219. Moore C, Movia D, Smith RJ, Hanlon D, Lebre F, Lavelle EC, Byrne HJ, Coleman JN, Volkov Y, McIntyre J (2017) Industrial grade 2D molybdenum disulphide (MoS_2): an in vitro exploration of the impact on cellular uptake, cytotoxicity, and inflammation. 2d Mater 4(2):025065. https://doi.org/10.1088/2053-1583/aa673f
220. Goldman EB, Zak A, Tenne R, Kartvelishvily E, Levin-Zaidman S, Neumann Y, Stiubea-Cohen R, Palmon A, Hovav AH, Aframian DJ (2015) Biocompatibility of tungsten disulfide inorganic nanotubes and fullerene-like nanoparticles with salivary gland cells. Tissue Eng Part A 21(5–6):1013–1023. https://doi.org/10.1089/ten.TEA.2014.0163
221. Wu X, Tian X, Chen T, Zeng A, Yang G (2018) Inorganic fullerene-like molybdenum selenide with good biocompatibility synthesized by laser ablation in liquids. Nanotechnology 29(29):295604. https://doi.org/10.1088/1361-6528/aac1b1
222. Teo Wei Z, Chng Elaine Lay K, Sofer Z, Pumera M (2014) Cytotoxicity of exfoliated transition-metal dichalcogenides (MoS_2, WS_2, and WSe_2) is lower than that of graphene and its analogues. Chem Eur J 20(31):9627–9632. https://doi.org/10.1002/chem.201402680
223. Chng ELK, Pumera M (2015) Toxicity of graphene related materials and transition metal dichalcogenides. RSC Adv 5(4):3074–3080. https://doi.org/10.1039/c4ra12624f
224. Latiff N, Teo WZ, Sofer Z, Huber S, Fisher AC, Pumera M (2015) Toxicity of layered semiconductor chalcogenides: beware of interferences. RSC Adv 5(83):67485–67492. https://doi.org/10.1039/c5ra09404f
225. Latiff NM, Teo WZ, Sofer Z, Fisher AC, Pumera M (2015) The cytotoxicity of layered black phosphorus. Chem Eur J 21(40):13991–13995. https://doi.org/10.1002/chem.201502006
226. Chia HL, Latiff NM, Sofer Z, Pumera M (2018) Cytotoxicity of group 5 transition metal ditellurides (MTe_2; M = V, Nb, Ta). Chem Eur J 24(1):206–211. https://doi.org/10.1002/chem.201704316
227. Rosli NF, Mayorga-Martinez CC, Latiff NM, Rohaizad N, Sofer Z, Fisher AC, Pumera M (2018) Layered $PtTe_2$ matches electrocatalytic performance of Pt/C for oxygen reduction reaction with significantly lower toxicity. ACS Sustain Chem Eng 6(6):7432–7441. https://doi.org/10.1021/acssuschemeng.7b04920

228. Yu Y, Yi Y, Li Y, Peng T, Lao S, Zhang J, Liang S, Xiong Y, Shao S, Wu N, Zhao Y, Huang H (2018) Dispersible MoS_2 micro-sheets induced a proinflammatory response and apoptosis in the gills and liver of adult zebrafish. RSC Adv 8(32):17826–17836. https://doi.org/10.1039/c8ra00922h
229. Hao J, Song G, Liu T, Yi X, Yang K, Cheng L, Liu Z (2017) In vivo long-term biodistribution, excretion, and toxicology of pegylated transition-metal dichalcogenides MS_2 (M = Mo, W, Ti) nanosheets. Adv Sci 4(1):1600160. https://doi.org/10.1002/advs.201600160

Linji Gong received his Bachelor's degree in chemistry from Nanchang University in China in 2015. He is currently a graduate student under the supervision of Prof. Yuliang Zhao and Prof. Zhanjun Gu at CAS key Laboratory for Biomedical Effects of Nanomaterials and Nanosafety, Institute of High Energy Physics, Chinese Academy of Sciences. He is now studying the synthesis of nanomaterials and exploring their biosafety and biomedical applications.

Zhanjun Gu received his B.E. degree (2002) from Huazhong University of Science and Technology and his Ph.D. degree (2007) from the Institute of Chemistry, Chinese Academy of Science, under the direction of Prof. Jiannian Yao. He then became a Postdoctoral Fellow at the University of Georgia. In 2009, he joined the faculty at CAS Key Lab for Biomedical Effects of Nanomaterials and Nanosafety, Institute of High Energy Physics, Chinese Academy of Science. His current research interests include nanomaterials synthesis, optical spectroscopy, and bioapplications of nanomaterials.